Acoustics of multiscale sorptive porous materials

R. Venegas,[1, a)] C. Boutin,[1, b)] and O. Umnova[2, c)]

[1)] *Université de Lyon - Ecole Nationale des Travaux Publics de l'Etat - LGCB/LTDS - UMR-CNRS 5513, Rue Maurice Audin, 69518 Vaulx-en-Velin, France.*

[2)] *Acoustics Research Centre, University of Salford, 43 Crescent, M54WT Salford, United Kingdom.*

(Dated: 11 June 2017)

This paper investigates sound propagation in multiscale rigid-frame porous materials that support mass transfer processes, such as sorption and different types of diffusion, in addition to the usual visco-thermo-inertial interactions. The two-scale asymptotic expansion method of homogenization for periodic media is successively used to derive the macroscopic equations describing sound propagation through the material. This allowed us to conclude that the macroscopic mass balance is significantly modified by sorption, inter-scale (micro- to/from nanopore scales) mass diffusion, and inter-scale (pore to/from micro- and nanopore scales) pressure diffusion. This modification is accounted for by the dynamic compressibility of the effective saturating fluid that presents atypical properties that lead to slower speed of sound and higher sound attenuation, particularly at low frequencies. Contrarily, it is shown that the physical processes occurring at the micro-nano scale do not affect the macroscopic fluid flow through the material. The developed theory is exemplified by introducing an analytical model for multiscale sorptive granular materials that is experimentally validated by comparing its predictions with acoustic measurements on granular activated carbon. Furthermore, we provide empirical evidence supporting an alternative method for measuring sorption and mass diffusion properties of multiscale sorptive materials using sound waves.

[a)] rodolfogustavo.venegascastillo@entpe.fr

[b)] claude.boutin@entpe.fr

[c)] o.umnova@salford.ac.uk

I. INTRODUCTION

Sound propagation in sorptive porous materials with multiple scales of heterogeneities, i.e. multiscale sorptive porous materials, is investigated in this paper. Sorption is a general term used to refer to adsorption, desorption, and absorption (penetration of the fluid into the solid phase). The former is a physical or chemical process in which the fluid molecules are adhered on to a surface. Adsorption can also be understood as an increase of fluid density in the vicinity of a fluid-solid interface. Desorption is the opposite phenomenon, i.e. the fluid molecules are released from a surface. The molecules adherence in physical adsorption is caused by weak van der Waals forces, while their release by either an increase of temperature or a decrease in pressure which leads to a break of the weak physical bond[1]. Adsorption/desorption is accompanied by mass diffusion that governs the flux of molecules from a region of higher concentration to one of lower concentration[1].

The microstructure of multiscale sorptive materials features pores or inclusions of very dissimilar characteristic sizes ranging from nanometers to millimeters. An example of this type of materials is a packing of porous grains in which the grains themselves feature two scales of heterogeneities, i.e. a triple porosity sorptive material. It will be demonstrated in this paper that their distinctive characteristic is the simultaneous occurrence of sorption processes at the smallest scale, different inter-scale diffusion processes, and visco-thermal effects at different scales. Materials of interest that possess hierarchical microstructure and support the mentioned physical processes include activated carbons[2], zeolites[3], and metal-organic frameworks[4], for example, in granular and pellet form.

The investigation of mass transport and sorption in multiscale porous materials is of interest, for example, in geophysics and gas engineering. For instance, in Ref. 5 the solute transport in fractured sorptive porous media was investigated. In Ref. 6, gas filtration in porous coal and the effect of gas constrained in nanometric pores was studied with the aim of understanding the physical mechanisms leading to coal-gas outbursts in coal mines. In Ref. 7, a dynamic model for mass transfer in coal seams with application to CO2 sequestration was investigated, while Ref. 8 dealt with the behavior of gas flow in multi-porosity shale gas reservoirs.

On the other hand, multiscale sorptive porous materials are widely used in chemical engineering applications such as filtration, gas storage, and catalysis, among others[1–4,9]. For

these applications, it is of interest to assess the sorption and diffusion properties of the materials. A measurement method, called frequency response[10–12], has been used to this end. This method aims at measuring the mass diffusion and sorption parameters of porous materials and is based on periodically perturbing the equilibrium of a system. For example, in a batch system it is normally considered a slow periodic change in volume of a container in which the sorptive material is placed. This change in volume leads to a slow periodic change in pressure that is recorded and further used to obtain the material parameters by fitting a theoretical model to the data. Of these models, the ones described in Refs. 13–15 for bidispersed structured sorbents are relevant to the present work. Their common features are: (i) the mass transport in both pore networks is modeled as a Fickian diffusion process, (ii) equilibrium between fluid and sorbed phases in the pores and linear isotherms are considered, and (iii) they are usually applied to describe diffusion and sorption in granular materials made by agglomerating porous microparticles (or crystals). In particular, the justification of (i) is the experimental condition normally used in the frequency response method: the measurements are taken at low pressures. At normal conditions, the mass transport in the pores formed in between millimeter-size inclusions is not of diffusive but advective type. This has been accounted for in Refs. 16 and 17 where sound propagation in a slit pore formed between two infinite nanoporous sorptive plates and in an array of cylindrical pores embedded in a nanoporous sorptive matrix were theoretically investigated, respectively. These works aimed at extending the working frequency range of the frequency response method and the structures studied can be considered as single-pore and double porosity sorptive materials.

In acoustics, the influence of sorption on sound propagation in a single tube has been investigated in Refs. 18 and 19. The main conclusion in Ref. 19 is that the contribution to sound energy dissipation due to viscosity, heat transfer, and mass diffusion are additive. Experimental work on the acoustical properties of granular activated carbon (GAC) has evidenced that partially filling a loudspeaker enclosure[20] or a Helmholtz resonator cavity[21] with GAC leads to an increase of their effective compliance. In addition, it has been shown that rigidly-backed layers of GAC display unusually large low frequency sound absorption coefficient[21–23]. The characteristic feature of activated carbons is that the low-frequency effective compressibility of the saturating gas attains values larger than the isothermal one predicted by the current theory of acoustics of porous media[23]. It was suggested in Ref. 23

that this behavior may be explained by considering an additional scale to the double porosity model introduced therein, as well as by accounting for sorption processes. This idea was developed further in Ref. 24 where rarefied gas flow in pores with size comparable to the molecular mean free path and sorption effects in nanopores were included into a model for sound propagation in granular activated carbon. One of the limitations of this model is that the inter-scale (inner-grain micro to/from nano pores) mass diffusion was assumed quasi-static. Hence, the model cannot be used to assess the influence of dynamic inter-scale mass diffusion on the acoustical properties of triple porosity sorptive materials. Furthermore, since this model was introduced in a phenomenological manner, its range of validity is not clearly identified. Recently, an upscaled model for sound propagation in double porosity sorptive materials has been developed in Ref. 25. This model cannot be used to describe the acoustical properties of triple porosity sorptive materials. The limitations of these two works are overcome in this paper. The aim is to describe the acoustical properties of a wide class of sorptive porous materials.

The first objective of this paper is to present a rigorous derivation of the macroscopic description of sound propagation in multiscale sorptive porous materials by making successive use of the two-scale asymptotic method of homogenization for periodic media[26,27]. The application of this method leads to an upscaled model whose range of validity is clearly identified. The upscaled model accounts for viscosity and heat transfer effects at the pore scale, rarefied gas flow and heat transfer at the micropore scale, inter-scale (pore to/from micro-nanopore scales) pressure diffusion, inter-scale (micro- to/from nanopore scales) mass diffusion, and sorption at the nanopore scale. The developed theory applies to materials saturated with a pure gas. Typical examples may be the system nitrogen/granular activated carbon, zeolites or metal-organic frameworks, which could approximate the acoustic behavior of this type of materials saturated with air.

The second objective of this paper is to determine the combined influence of sorption, rarefaction, and dynamic inter-scale diffusion processes on sound propagation through triple porosity sorptive materials. Crucially, it is demonstrated that sorption effects occurring in pores of nanometer size strongly modify the macroscopic mass balance. This modification is accounted for by the compressibility of the effective saturating fluid, which displays unconventional properties that result in a slower speed of sound and higher attenuation of sound in the material. The strength of these macroscopic effects in the audible frequency range

largely depends on the dynamic pressure and mass diffusion properties of the material. This cannot be properly assessed using the models developed in Refs. 24 and 25 due to their limitations discussed above. Contrarily to sorption effects, it is shown that the effects of rarefied gas flow in pores with size comparable to the molecular mean free path only intervene in the macroscopic acoustic behavior indirectly via a modification of the apparent pressure diffusivity. Furthermore, it is proven that, under the conditions established by homogenization and in coherence with our previous studies[23,24], the constitutive fluid flow law and its associated effective parameter, i.e. the dynamic viscous permeability, are not modified by the physical processes occurring in the micro and nano pores.

The strong combined influence of sorption and mass diffusion on the acoustical properties of the materials is measurable. Hence the third objective of this paper corresponds to the use of acoustic measurements on macroscopic samples to deduce physical parameters characterizing sorption, that occurs at the nanoscale, and the effective diffusivity determining the inter-scale mass diffusion. This may provide a simple alternative procedure to measure the sorption and diffusion properties of multiscale sorptive materials. We provide empirical evidence supporting this claim and validate the developed theory experimentally.

The paper is organized as follows. The macroscopic description of sound propagation in multiscale sorptive porous materials is presented in Section II. The analysis of the effective parameters of the upscaled model follows. An analytical model for sound propagation in multiscale sorptive granular material is introduced in Section IV. This is further used in Section V to exemplify and experimentally validate the theory. The main findings are summarized in the conclusions.

II. SOUND PROPAGATION IN MULTISCALE SORPTIVE POROUS MATERIALS - THEORY

This section deals with the derivation of the macroscopic equations that describe sound propagation in multiscale sorptive porous materials. The upscaling is done using the two-scale asymptotic method of homogenization for periodic media[26,27]. The material geometry and the main assumptions regarding its morphology are discussed first. We then focus on the case of a multiscale sorptive material with well separated macro, meso, micro and nano scales. This allows applying the upscaling method to the set of equations that describes

the acoustic behavior in the pore fluid network, where viscosity and heat transfer effects take place, and in the micro-nano porous domain. The latter is modeled as an equivalent continuum and accounts for viscosity and heat transfer effects at the micropore scale, inter-scale mass diffusion characterized by the micropore geometry and two diffusion processes (i.e. bulk and surface diffusion) occurring in the nanopores, and sorption on the walls of the nanopores. The effective equations governing sound propagation in the micro-nano porous domain have been derived in Ref. 25. We present in Appendix A the main steps of the derivation as well as its extension to account for rarefied gas flow and heat transfer in pores with size comparable to the molecular mean free path.

A. Geometry

Consider a periodic multiscale sorptive rigid-frame porous material saturated with a pure Newtonian fluid. Figure 1 shows a diagram of the scales of the material and the relevant geometrical descriptors. The macroscopic characteristic length L is related to the sound wavelength λ through $L = |\lambda|/2\pi$ and strongly exceeds all other characteristic lengths of the material. The representative elementary volume (REV) of the material is denoted as Ω_p. This is constituted by the volume of the pores Ω_{pf} and the volume of the micro-nano porous domain Ω_{mn}, i.e. $\Omega_p = \Omega_{pf} \cup \Omega_{mn}$. The solid part of Ω_{mn} is assumed perfectly impervious to gas transport. The surface of the pores is denoted as Γ_p. The micro-nano porous domain Ω_{mn} has a REV Ω_m that comprises the volume of the micropores Ω_{mf} and that of the nano porous domain Ω_n, i.e. $\Omega_m = \Omega_{mf} \cup \Omega_n$. The surface of the micropores is denoted as Γ_m. In turn, the nano porous domain is composed of the volume of the nanopores Ω_{nf} and the volume of its impervious solid part. The surface of the nanopores is represented by Γ_n.

The characteristic length associated with the pore (or the period of the material), micropore, and nanopore scales are denoted as l_p, l_m, and l_n, respectively. These are well separated, i.e. $l_n << l_m << l_p$, and for the materials of interest are usually millimetric, micrometric, and nanometric in size (see e.g. Ref. 9).

Because of the separation between the pore and micropore scales, i.e. $l_m/l_p << 1$, the micro-nano porous domain Ω_{mn} can be modeled as an equivalent continuum[28]. Similarly, since the characteristic size associated with the nanopore scale is much smaller than that associated with the micropore scale, i.e. $l_n/l_m << 1$, the nano porous domain can be

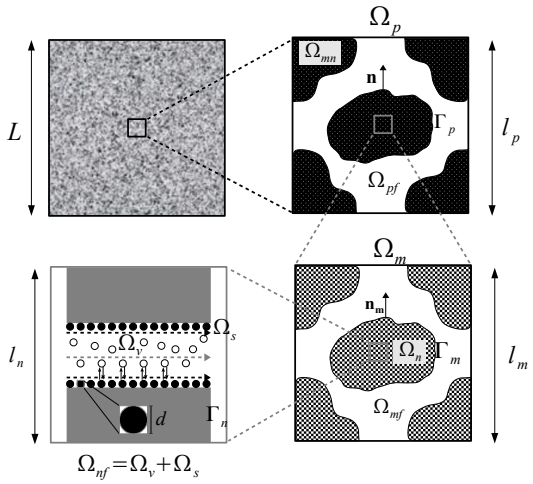

FIG. 1. Diagram of the scales of a multiscale sorptive porous material.

considered as an equivalent continuum governed by effective equations that are defined in the whole domain Ω_n and reflect the following local physical processes[25]: sorption occurring on the walls of the nanopores, volumetric diffusion of free gas molecules in the bulk of the nanopores, and surface diffusion of the adsorbed molecules. The diffusion processes are respectively represented in Figure 1 by the horizontal dashed gray and black lines, while the mass exchange between the gas (hollow circles) and adsorbate (black circles) phases is depicted with vertical lines with arrows. The adsorbate volume is estimated by $\Omega_s = |\Gamma_n| N d$, where N is the number of adsorbed layers and d is the diameter of the molecules. These are respectively assumed equal to unity (i.e. $N = 1$, monolayer coverage) and smaller than the nanopore characteristic size (i.e. $d < l_n$). The void space available for the transport of free molecules is represented by Ω_v. Hence one has that $\Omega_{nf} = \Omega_v \cup \Omega_s$.

The porosity of the material is $\phi_{pmn} = \phi_p + (1-\phi_p)(\phi_m + (1-\phi_m)\phi_n)$, where $\phi_p = \Omega_{pf}/\Omega_p$, $\phi_m = \Omega_{mf}/\Omega_m$, and $\phi_n = \Omega_{nf}/\Omega_n$ are the porosities associated with the pores, micropores, and nanopores, respectively. In turn, the porosity of the pores and micropores is $\phi_{pm} = \phi_p + (1-\phi_p)\phi_m$, while that of the micro-nano porous domain is $\phi_{mn} = \phi_m + (1-\phi_m)\phi_n$.

The disparity in length scales between the pore size and the macroscopic characteristic size associated with the acoustic phenomenon provides a small parameter $\epsilon = l_p/L << 1$.

B. Governing equations at the pore scale

The equations describing sound propagation in the pore fluid network are[29–32]: the linearized equations of conservation of momentum (1), mass (2), and energy (3); and the equation of state (4). The physical parameters involved are the dynamic viscosity η, specific heat capacity C_p, thermal conductivity κ, and equilibrium pressure P_0, density ρ_0, and temperature τ_0. The oscillating velocity, pressure, density, and temperature are denoted as $\mathbf{u}_p$, p_p, ρ_p, and τ_p, respectively. Note that harmonic dependence of the type $e^{j\omega t}$ is assumed and, because of linearity, this term is omitted throughout the paper.

$$\eta\nabla^2\mathbf{u}_p - \nabla p_p = j\omega\rho_0\mathbf{u}_p \quad \text{in} \quad \Omega_{pf}, \tag{1}$$

$$j\omega\rho_p + \rho_0\nabla\cdot\mathbf{u}_p = 0 \quad \text{in} \quad \Omega_{pf}, \tag{2}$$

$$\kappa\nabla\cdot\nabla\tau_p = j\omega C_p\rho_0\tau_p - j\omega p_p \quad \text{in} \quad \Omega_{pf}, \tag{3}$$

$$\frac{p_p}{P_0} = \frac{\rho_p}{\rho_0} + \frac{\tau_p}{\tau_0} \quad \text{in} \quad \Omega_{pf}. \tag{4}$$

The equations governing sound propagation in the micro-nano porous domain, which is modeled as an equivalent continuum, have been derived in Ref. 25 for the case of negligible rarefaction effects in the micropores. We extend this model in Appendix A to account for these effects. The derived effective equation of conservation of mass (5) and dynamic Darcy's law (6) are given by:

$$\nabla\cdot\mathbf{U}_m + j\omega p_m\mathsf{C}_{mn}(\omega) = 0 \quad \text{in} \quad \Omega_{mn}, \tag{5}$$

$$\mathbf{U}_m = -\frac{\mathbf{k}_m(\omega)}{\eta}\cdot\nabla p_m \quad \text{in} \quad \Omega_{mn}, \tag{6}$$

where p_m is pressure in the micropores, $\mathbf{U}_m$ is the Darcy's velocity, $\mathbf{k}_m(\omega)$ is the dynamic viscous permeability associated with the micropores and $\mathsf{C}_{mn}(\omega)$ is the compressibility of the effective fluid saturating the micro-nano porous domain (hence the subscript mn). Explicit expressions for the latter two parameters will be given further below.

Eqs. (1)-(6) are coupled via the following conditions on the pore boundary Γ_p expressing the continuity of normal mass flux (7) and pressure (8), and of negligible temperature variations (9). Note that $\mathbf{n}$ is the outward-pointing normal vector (see Figure 1).

$$\rho_0\mathbf{u}_p\cdot\mathbf{n} = \rho_0\mathbf{U}_m\cdot\mathbf{n} \quad \text{on} \quad \Gamma_p, \tag{7}$$

$$p_p = p_m \quad \text{on} \quad \Gamma_p, \tag{8}$$

$$\tau_p = 0 \quad \text{on} \quad \Gamma_p. \tag{9}$$

Together with the boundary condition (7), it is set that the tangential mass flux is zero, i.e. $\rho_0(\mathbf{u}_p - (\mathbf{u}_p \cdot \mathbf{n})\mathbf{n}) = \mathbf{0}$. In addition, by considering the continuity of heat flux and its estimation[33] $\kappa\tau_p/l_p = \kappa\tau_m/l_m$, one obtains $\tau_m = l_m\tau_p/l_p$. Then, the variation of temperature in the pores is much larger than that in the micropores, i.e. $\tau_p >> \tau_m$, and the condition Eq. (9) is thereby justified.

C. Homogenization procedure

The scale separation between the pore and macroscopic characteristic sizes, i.e. $l_p/L = \epsilon << 1$, allows us to use the two-scale asymptotic expansion method of homogenization for periodic media to derive an equivalent macroscopic model. To represent the evolution at the two spatial scales, the following dimensionless space variables $\mathbf{x}/L = \boldsymbol{x}^*$ and $\mathbf{x}/l_p = \boldsymbol{y}^*$ are introduced, where $\mathbf{x}$ stands for the usual space variable. These dimensionless space variables are associated with the variations at the local and macroscopic scales, respectively. Equivalently, taking L as reference length, we will use the following two dimensional space variables $\boldsymbol{x} = L\boldsymbol{x}^*$ and $\boldsymbol{y} = L\boldsymbol{y}^* = \boldsymbol{x}L/l_p = \varepsilon^{-1}\boldsymbol{x}$. Then, the usual gradient operator ∇ is given by $\nabla_{(xy)} = \nabla_x + \varepsilon^{-1}\nabla_y$ (and $\nabla^2_{(xy)} = \nabla^2_x + 2\varepsilon^{-1}\nabla_{xy} + \varepsilon^{-2}\nabla^2_y$). Note that for simplicity in the notation, we have used non-bold letters for the spatial variables.

The use of two space variables should be combined with a rescaling of the usual equations based upon a single space variable. The reason for the rescaling lies in the fact that when expressed with the two space variables (x, y), the actual physical gradient of a quantity Q that varies at the macroscopic scale, i.e. $\nabla_x Q$, becomes $\nabla_{(xy)}Q$. Similarly, if the quantity varies at the local scale, the actual physical gradient $\nabla_y Q$ reads $\varepsilon\nabla_{(xy)}Q$. Therefore, the gradient of variables oscillating at the local scale should be rescaled. In other words, to formulate the set of rescaled equations governing sound propagation at the pore scale one should analyze at which scale the physical quantities fluctuate as well as the relative order of magnitude of the terms in the governing equations. This analysis for the variables and terms in Eqs. (1)-(4) is well established. The arguments and procedure can be found, for example, in Refs. 27 and 30 and are now recalled.

In the long-wavelength regime the pore pressure fluctuates at the macroscopic scale, i.e.

$|\nabla p_p| = O(p_p/L)$ and, while the fluid velocity and its rate of deviatoric deformation vary at the pore scale (i.e. $|\eta\nabla^2\mathbf{u}_p| = O(\eta u_p/l_p^2)$), the microscopic divergence itself is of the order of the macroscopic divergence, i.e. $|\nabla\cdot\mathbf{u}_p| = O(u_p/L)$. Note that, for example, u_p is an estimation of $|\mathbf{u}_p|$. On the other hand, the temperature varies at the pore scale, which leads to the following estimation $|\kappa\nabla^2\tau_p| = O(\kappa\tau_p/l_p^2)$. Regarding the relative order of magnitude, we are interested in the case when the viscous and inertial terms in the oscillatory Stokes equation (1) balance the pressure gradient. Hence the estimations of the three terms in Eq. (1) are of the same order of magnitude, i.e. $O(\eta u_p/l_p^2) = O(\omega\rho_0 u_p) = O(p_p/L)$. Similarly, the estimations of the three terms in the equation of conservation of energy (3) are of the same order of magnitude, i.e. $O(\kappa\tau_p/l_p^2) = O(\omega\rho_0 C_p\tau_p) = O(\omega p_p)$. Furthermore, the estimation of the terms in the equations of conservation of mass and of state satisfy $O(u_p/L) = O(\omega\rho_p/\rho_0)$ and $O(p_p/P_0) = O(\rho_p/\rho_0) = O(\tau_p/\tau_0)$, respectively.

In the micro-nano porous domain, both the Darcy's velocity $\mathbf{U}_m$ and the micropore pressure p_m fluctuate at the pore scale. In addition, the estimations of the terms in the mass balance equation (5), as well as those in the dynamic Darcy's law Eq. (6)), are of the same order of magnitude: $O(U_m/l_p) = O(\omega p_m C_{mn})$ and $O(U_m) = O(\mathcal{K}_m p_m/\eta l_p)$.

Regarding the boundary conditions, the continuity of pressure on the pore boundaries Γ_p sets $O(p_p) = O(p_m)$ while the long-wavelength condition imposes that the advective mass flux pulsed from the micro-nano porous domain on Γ_p is of one order smaller than the advective mass flux generated by the incident wave in the pores, i.e.

$$\mathcal{U} = \frac{|\rho_0\mathbf{U}_m\cdot\mathbf{n}|}{|\rho_0\mathbf{u}_p\cdot\mathbf{n}|} = O(\epsilon). \tag{10}$$

This estimate is justified by the following argument. Consider a cell Ω and denote the ingoing mass flux on one face (of surface S) as $S\rho_0 u_{p_1}$, the outgoing mass flux on the opposite face as $S\rho_0 u_{p_2}$, and the mass flux pulsed from the micro-nano porous domain Ω_{mn} as $\rho_0 U_m\Gamma_p$. By hypothesis, a regime of long wavelength $L >> l$ is considered. Thus, $(S\rho_0 u_{p_2} - S\rho_0 u_{p_1})/S\rho_0 u_{p_1} \approx l_p/L$. Since from conservation of mass $S\rho_0 u_{p_2} \approx S\rho_0 u_{p_1} + \Gamma_p\rho_0 U_m$, it follows that $\Gamma_p\rho_0 U_m/S\rho_0 u_{p_1} \approx l_p/L = \epsilon$.

In terms of physical parameters, the ratio between the mass fluxes on the pore boundary Γ_p can be written as:

$$\mathcal{U} = \frac{|\rho_0\mathbf{U}_m\cdot\mathbf{n}|}{|\rho_0\mathbf{u}_p\cdot\mathbf{n}|} = \frac{\mathcal{K}_m p_m}{\eta l_p}\frac{\eta L}{l_p^2 p_p} = \frac{\mathcal{K}_m}{l_p^2}\frac{L}{l_p} = \frac{l_m^2}{l_p^2}\epsilon^{-1} = O(\epsilon). \tag{11}$$

Note that i) the continuity of pressure on Γ_p (i.e. Eq. (8)) has been used and ii) the estimation (11) holds as long as characteristic sizes associated with the pore and micropore scales are well separated, i.e. $l_m/l_p = O(\epsilon)$. Analogously, this condition can be expressed in terms of the viscous permeabilities associated with the pore and micropore fluid networks as $\mathcal{K}_m/\mathcal{K}_p = O(\epsilon^2)$, i.e. the permeabilities are highly contrasted. Furthermore, the mass flux ratio estimation is consistent with the modeling of the micro-nano porous domain as an equivalent continuum.

The rescaled set of equations describing sound propagation at the pore scale is then given by Eqs. (12)-(19). Note that we adopt the usual homogenization convention that consists in keeping the same notation as for the single-space-variable formulation for both the variables and the gradient operator. For example, ∇ and $\mathbf{u}_p$ stand for $\nabla_{(xy)}$ and $\mathbf{u}_p(x,y)$, respectively.

$$\epsilon^2\eta\nabla^2\mathbf{u}_p - \nabla p_p = j\omega\rho_0\mathbf{u}_p \quad \text{in} \quad \Omega_{pf}, \tag{12}$$

$$j\omega\left(\frac{p_p}{P_0} - \frac{\tau_p}{\tau_0}\right) + \nabla\cdot\mathbf{u}_p = 0 \quad \text{in} \quad \Omega_{pf}, \tag{13}$$

$$\epsilon^2\kappa\nabla\cdot\nabla\tau_p = j\omega C_p\rho_0\tau_p - j\omega p_p \quad \text{in} \quad \Omega_{pf}, \tag{14}$$

$$\epsilon\nabla\cdot\mathbf{U}_m + j\omega p_m\mathsf{C}_{mn} = 0 \quad \text{in} \quad \Omega_{mn}, \tag{15}$$

$$\mathbf{U}_m = -\frac{\mathbf{k}_m}{\eta}\cdot\epsilon\nabla p_m \quad \text{in} \quad \Omega_{mn}. \tag{16}$$

$$\rho_0\mathbf{u}_p\cdot\mathbf{n} = \epsilon\rho_0\mathbf{U}_m\cdot\mathbf{n} \quad \text{on} \quad \Gamma_p, \tag{17}$$

$$p_m = p_p \quad \text{on} \quad \Gamma_p, \tag{18}$$

$$\tau_p = 0 \quad \text{on} \quad \Gamma_p. \tag{19}$$

The physical variables are then looked for in the form of asymptotic expansions in powers of the small parameter $\epsilon = l_p/L$ as $Q(x,y) = \sum_{i=0}^{\infty}\epsilon^i Q^{(i)}(x,y)$ where $Q = p_p, \mathbf{u}_p, \tau_p, \rho_p, p_m, \mathbf{U}_m$. These are then replaced in Eqs. (12)-(19) and the terms of the same order are identified. This leads to cell problems whose solutions are used in conjunction with the leading-order mass balance equation spatially averaged over the pore volume to obtain the macroscopic equations that describe sound propagation in multiscale sorptive porous materials introduced in the next section. The mathematical details of the derivation are presented in Appendix B.

D. Macroscopic description of sound propagation in multiscale sorptive materials

The macroscopic mass balance equation and fluid flow constitutive law determining sound propagation in multiscale sorptive porous materials are a key result of this paper and are respectively given by Eqs. (20) and (21) (see Appendix B for their derivation).

$$\nabla_x \cdot \langle \mathbf{u}_p^{(0)} \rangle + j\omega p_p^{(0)} \mathsf{C}(\omega) = 0, \tag{20}$$

$$\langle \mathbf{u}_p^{(0)} \rangle = -\frac{\mathbf{k}(\omega)}{\eta} \cdot \nabla_x p_p^{(0)}. \tag{21}$$

Here the dynamic viscous permeability tensor is given by $\mathbf{k}(\omega) = \mathbf{k}_p(\omega)$, with $\mathbf{k}_p(\omega)$ being the dynamic viscous permeability tensor associated with the pore fluid network. The effective dynamic compressibility $\mathsf{C}(\omega)$ is given by Eq. (22) and corresponds to the sum of the classical effective dynamic compressibility $\mathsf{C}_p(\omega)$ (Eq. (23)) that accounts for heat transfer in the pores and an additional effective dynamic compressibility $\mathsf{C}_{mn}(\omega)$ that results from the mechanisms of heat transfer in the micropores, inter-scale (micro-nano) mass diffusion, and sorption in the nanopores. The contribution of $\mathsf{C}_{mn}(\omega)$ is weighted by the function $\mathcal{F}_{pmn}(\omega)$, which accounts for inter-scale pressure diffusion effects.

$$\mathsf{C}(\omega) = \mathsf{C}_p(\omega) + (1-\phi_p)\mathsf{C}_{mn}(\omega)\mathcal{F}_{pmn}(\omega). \tag{22}$$

The dynamic compressibility C_p of the effective fluid saturating the pore network is given by:

$$\mathsf{C}_p(\omega) = \frac{\phi_p}{P_0}\left(1 - \frac{j\omega}{\omega_{tp}}\frac{\gamma-1}{\gamma}\frac{\Theta_p(\omega)}{\Theta_{p0}}\right), \tag{23}$$

where $\Theta_p(\omega)$ is the dynamic thermal permeability associated with the pore fluid network and the thermal characteristic frequency determining the transition from isothermal to adiabatic sound propagation in the pore fluid network is defined as $\omega_{tp} = \kappa\phi_p/\rho_0 C_p \Theta_{p0}$, where $\Theta_{p0} = \Theta_p(\omega = 0)$ is the static thermal permeability[32].

The function $\mathcal{F}_{pmn}$ is given by:

$$\mathcal{F}_{pmn}(\omega) = 1 - \frac{j\omega}{\omega_b}\frac{\mathcal{B}_{app0}}{\mathcal{B}_{app}}\frac{B(\omega)}{B_0}, \tag{24}$$

where $B(\omega)$ is the inter-scale pressure diffusion function, $\mathcal{B}_{app} = \mathcal{K}_m/\eta\mathsf{C}_{mn}$ is the apparent pressure diffusivity, and the pressure diffusion characteristic frequency is estimated as $\omega_b =$

$(1-\phi_p)\mathcal{B}_{app0}/B_0$. Here $B_0 = B(\omega = 0)$ is the static value of the inter-scale pressure diffusion function, $\mathcal{B}_{app0} = \mathcal{K}_{m0}/\eta \mathsf{C}_{mn0}$ is the static apparent pressure diffusivity, $\mathcal{K}_{m0} = \mathcal{K}_m(\omega = 0)$ is the static viscous permeability associated with the micropore fluid network, and $\mathsf{C}_{mn0} = \mathsf{C}_{mn}(\omega = 0)$.

The dynamic compressibility of the effective fluid saturating the micro-nano porous domain $\mathsf{C}_{mn}(\omega)$ is given by (see Appendix A for its derivation):

$$\mathsf{C}_{mn}(\omega) = \mathsf{C}_m(\omega) + (1 - \phi_m)\mathsf{C}_n\mathcal{F}_{mn}(\omega), \tag{25}$$

where the dynamic compressibility of the effective fluid saturating the micropores C_m is calculated using Eq. (23) with the subscript p being replaced by m. The effective compressibility of the nano porous domain C_n and the function $\mathcal{F}_{mn}$ that accounts for inter-scale (micro-nano) mass diffusion are given by:

$$\mathsf{C}_n = \frac{H_e}{P_0}, \tag{26}$$

$$\mathcal{F}_{mn}(\omega) = 1 - \frac{j\omega}{\omega_d}\frac{G(\omega)}{G_0}, \tag{27}$$

where the mass diffusion characteristic frequency is defined as $\omega_d = (1 - \phi_m)\mathcal{D}_{app}/G_0$. Here G_0 is the static value of the dynamic inter-scale mass diffusion $G(\omega)$ (see Eq. (A.35)), $\mathcal{D}_{app} = D_e/H_e$ is the apparent mass diffusivity, D_e is the effective diffusion coefficient, and H_e is the effective linearized sorption equilibrium constant[25]. Note that D_e can be expressed in terms of the diffusion coefficients associated with the volumetric diffusion of free gas molecules in the bulk of the nanopores and surface diffusion of the adsorbed molecules on the walls of the nanopores (see Eq. (A.5)), while H_e in terms of the linearized sorption equilibrium constant H (see Eq. (A.6)) and can be related to the parameters of the classical Langmuir isotherm model[34] via Eq. (A.37).

Further assuming macroscopic isotropy, the dynamic viscous permeability becomes $\mathbf{k} = \mathcal{K}\mathbf{I}$, where $\mathbf{I}$ is the unitary second-rank tensor. Then, the characteristic impedance Z_c, wave number k_c, and speed of sound $\mathcal{C}$ in the material are given by[35] (with $\mathcal{K} = \mathcal{K}_p$):

$$Z_c(\omega) = \sqrt{\frac{\eta}{j\omega\mathcal{K}\mathsf{C}}} \quad , \quad k_c(\omega) = \omega\sqrt{\frac{\eta\mathsf{C}}{j\omega\mathcal{K}}} \quad , \quad \mathcal{C}(\omega) = \frac{\omega}{k_c(\omega)}. \tag{28}$$

Quantities that will be used to experimentally validate the theory are the surface impedance Z_w and sound absorption coefficient α of a rigidly-backed layer of material

of thickness d_l. These are given by:

$$Z_w(\omega) = -jZ_c \cot(k_c d_l), \quad \alpha(\omega) = 1 - \left| \frac{Z_w - Z_0}{Z_w + Z_0} \right|^2 = \frac{4X^*}{(1+X^*)^2 + (Y^*)^2}. \tag{29}$$

where $Z_0 = \rho_0 c_0$ is the characteristic impedance of the saturating fluid, c_0 its speed of sound, and $X^* = \mathrm{Re}(Z_w(\omega)/Z_0))$ and $Y^* = \mathrm{Im}(Z_w(\omega)/Z_0))$ are the normalized resistance and reactance, respectively.

In summary, the derived macroscopic equations (20) and (21) that describe sound propagation in multiscale sorptive rigid-frame porous materials allows us to conclude that the dynamic Darcy's law and the dynamic viscous permeability are not modified by the physical processes occurring in the micro-nano porous domain. Only the fluid flow in the pore fluid network influences the dynamic permeability values. Conversely, the effective dynamic compressibility becomes significantly modified by i) inter-scale pressure diffusion (pores to/from the micro-nano porous domain), ii) inter-scale mass diffusion (micropores to/from the nano porous domain), and iii) sorption occurring on the walls of the nanopores. This modification comes from the appearance of a source term in the macroscopic mass balance equation, i.e. the third term in Eq. (B.8), that accounts for the contribution of these physical processes. Since the quantities in Eqs. (28) and (29) depend on $\mathsf{C}(\omega)$, these are all modified by the physical processes that influence the effective dynamic compressibility.

III. ANALYSIS OF THE EFFECTIVE PARAMETERS

The limiting values of the effective dynamic compressibility $\mathsf{C}(\omega << \omega_{\min}) = \mathsf{C}_{lf}$ and $\mathsf{C}(\omega >> \omega_{\max}) = \mathsf{C}_{hf}$, where $\omega_{\min} = \min(\omega_{tp}, \omega_d, \omega_b, \omega_{tm})$ and $\omega_{\max} = \max(\omega_{tp}, \omega_d, \omega_b)$, are an important result of this paper. These are given by (see Appendix C for their derivation):

$$\mathsf{C}_{hf} P_0 = \frac{\phi_p}{\gamma}, \tag{30}$$

$$\mathsf{C}_{lf} P_0 = \phi_p + (1-\phi_p)(\phi_m + (1-\phi_m)H_e) - \frac{j\omega}{\omega_c}, \tag{31}$$

where ω_c is a global characteristic frequency that accounts for the thermal and diffusive processes in the material and is defined by:

$$\frac{1}{\omega_c} = \phi_p \frac{\gamma - 1}{\gamma} \frac{1}{\omega_{tp}} + (1-\phi_p)\phi_m \left(\frac{\gamma - 1}{\gamma} \frac{1}{\omega_{tm}} + \frac{1}{\omega_b} \right) + (1-\phi_p)(1-\phi_m) H_e \left(\frac{1}{\omega_b} + \frac{1}{\omega_d} \right). \tag{32}$$

Eq. (30) shows that for frequencies much higher than those characterizing the diffusion mechanisms, the influence of the physical processes occurring in the micro-nano porous domain on the macroscopic effective dynamic compressibility is negligible.

On the right-hand side of Eq. (32), the first term is associated with the effects of heat transfer between the solid frame and the fluid in the pores. The second term accounts for heat transfer between the solid frame and the fluid in the micropores and the influence of inter-scale pressure diffusion. The third term is associated with inter-scale pressure and mass diffusion. Note that sorption modifies both the mass diffusion- and pressure diffusion-related effects via the dependence of the respective characteristic frequencies on the effective linearized sorption equilibrium constant H_e. By construction one has that $\omega_{tp} < \omega_{tm}$, $\omega_d < \omega_{tm}$, and $\omega_b < \omega_{tm}$. Depending on the morphologies of the pore fluid network and micro-nano porous domain as well as their associated thermal and apparent mass diffusivities, the mass diffusion characteristic frequency could be either smaller, in the order of, or larger than the thermal characteristic frequency associated with the pore fluid network, i.e. either $\omega_d < \omega_{tp}$, $\omega_d = O(\omega_{tp})$, or $\omega_d > \omega_{tp}$. Similarly, the same type of sorting relationship can be observed for ω_b and ω_{tp}. On the other hand, one may observe $\omega_d = O(\omega_b)$ or $\omega_d > \omega_b$ for fast diffusing system, while for strongly sorptive gas-solid system presenting slow mass diffusion the inequality $\omega_d < \omega_b$ is likely to be observed.

Defining the ratio between the effective adsorbate concentration in the nanopores and the effective gas concentration in the pores and micropores as $M_H = (1-\phi_p)(1-\phi_m)H_e/\phi_{pm}$, it follows from Eq. (31) that the static compressibility is given by:

$$\mathsf{C}_0 = \mathsf{C}(\omega = 0) = \frac{1}{P_0}(\phi_p + (1-\phi_p)(\phi_m + (1-\phi_m)H_e) = \frac{1}{P_0}\phi_{pm}(1+M_H). \qquad (33)$$

This equation shows that, as a consequence of sorption, the low-frequency effective dynamic compressibility can attain a value substantially larger than that of conventional porous materials.

It is worth highlighting that the direct relation between the effective linearized sorption equilibrium parameter H_e and the real part of the low-frequency effective dynamic compressibility, given by Eq. (33), allows deducing H_e from measurements of $\mathrm{Re}(\mathsf{C}(\omega \to 0))$. On the other hand, the effective diffusion coefficient D_e can be measured from measurements of the imaginary part of the effective dynamic compressibility and the use of Eq. (31), provided that the other macroscopic parameters involved are known.

In general, the effective dynamic compressibility reduces to that of conventional single porosity non-sorptive materials when $\phi_n = \phi_m = 0$, i.e. $\mathsf{C}(\omega) = \mathsf{C}_p(\omega)$. Hence its limiting values are $P_0\mathsf{C}(\omega >> \omega_{tp}) = \phi_p/\gamma$ and $P_0\mathsf{C}(\omega << \omega_{tp}) = \phi_p - j\omega/\omega_c$, with $1/\omega_c$ being equal to the first term on the right-hand side of Eq. (32).

In absence of nanopores, i.e. $\phi_n = 0$ (or $H_e = 0$), the effective dynamic compressibility of double porosity non-sorptive materials with highly contrasted permeabilities[33,36] is retrieved, i.e. $\mathsf{C}(\omega) = \mathsf{C}_p + (1-\phi_p)\mathsf{C}_m(\omega)\mathcal{F}_{pm}(\omega)$. Here $\mathcal{F}_{pm}$ is calculated using Eq. (24) and keeping in mind that the apparent pressure diffusivity becomes $\mathcal{B}_{app} = \mathcal{B}_{app0} = \mathcal{K}_{m0}P_0/\phi_m\eta$. Consequently, the pressure diffusion characteristic frequency is given by $\omega_b = (1-\phi_p)\mathcal{K}_{m0}P_0/\phi_m\eta B_0$ and the limiting values of the effective dynamic compressibility are $P_0\mathsf{C}(\omega << \omega_{tp}) = \phi_{pm} - j\omega/\omega_c$ and $P_0\mathsf{C}(\omega >> \omega_b) = \phi_p/\gamma$. In this case, $1/\omega_c$ is given by Eq. (32) for $H_e = 0$.

The case of a material without micropores, i.e. $\phi_m = 0$, given the extremely large separation between the characteristic sizes associated with the nanopore and pore scales considered in this work, is of less interest since the mass flux pulsed from the nano porous domain is extremely small in comparison with the mass flux in the pores. Hence the mass flux ratio is estimated by $\mathcal{U} = O(\epsilon^2)$ and the material effectively behaves as a single porosity non-sorptive material in the audible frequency range.

For a material without mesoscopic pores, i.e. $\phi_p = 0$, the effective dynamic compressibility reduces to that of double porosity sorptive materials introduced in Ref. 25 (see also Appendix A), while the dynamic viscous permeability is given by $\mathcal{K} = \mathcal{K}_m$.

The case of pressure and mass diffusion occurring without sorption is observed when i) the number of adsorbed layers is equal to zero (i.e. $N = 0$), ii) the concentrations of the adsorbed and gaseous phases are identical (i.e. $H = 1$), or iii) the characteristic size of the nanopores is much larger than the size of the molecules, i.e. $l_n >> d$. In all these situations, the effective dynamic compressibility reduces to that of a triple-porosity non-sorptive material and is calculated using Eq. (22). The parameters involved take the values: $D_e = \phi_n D_n$, $H_e = \phi_n$, and $\mathcal{B}_{app} = \mathcal{K}_{m0}P_0/\phi_{mn}\eta$. Hence, one has that $P_0\mathsf{C}(\omega << \omega_{\min}) = \phi_{pmn} - j\omega/\omega_c$ and $P_0\mathsf{C}(\omega >> \omega_{\max})) = \phi_p/\gamma$, where $1/\omega_c$ is given by Eq. (32) with $H_e = \phi_n$.

As discussed previously, the fluid flow at the leading order remains unaffected by the physical processes occurring in the micro-nano porous domain under the conditions established through homogenization (i.e. $\mathcal{U} = O(\epsilon)$ and $\mathcal{J} = O(\varepsilon)$, see Eqs. (10) and (A.11)).

Hence the properties of the dynamic viscous permeability are the same as those of this parameter for single porosity non-sorptive materials. Considering leading-order terms only, the dynamic viscous permeability takes the following limiting values[31]: $\mathcal{K}(\omega << \omega_{vp}) = \mathcal{K}_0$ and $\mathcal{K}(\omega >> \omega_{vp}) = -j\phi_p\delta_v^2/\alpha_\infty$, where $\omega_{vp} = \phi_p\eta/\rho_0\mathcal{K}_0\alpha_\infty$ is the viscous characteristic frequency, $\delta_v = \sqrt{\eta/\rho_0\omega}$ is the viscous boundary layer thickness, and α_∞ is the tortuosity.

Using the asymptotic values of $\mathsf{C}(\omega)$ and $\mathcal{K}(\omega)$, the following limiting values for the speed of sound and wave number are obtained:

$$\begin{aligned}\mathcal{C}(\omega \to 0) &= \sqrt{\frac{j\omega\mathcal{K}_0}{\eta}\frac{P_0}{\phi_{pm}(1+M_H)}} = \frac{\mathcal{C}_{0\phi_p}}{\sqrt{\frac{\phi_{pm}}{\phi_p}(1+M_H)}} = \frac{\mathcal{C}_{0\phi_{pm}}}{\sqrt{1+M_H}} \\ &= \frac{\mathcal{C}_{0\phi_{pmn}}}{\sqrt{\frac{\phi_{pm}}{\phi_{pmn}}(1+M_H)}}, \\ \mathcal{C}(\omega \to \infty) &= \mathcal{C}_{\infty\phi_p} = \mathcal{C}_{\infty\phi_{pm}} = \mathcal{C}_{\infty\phi_{pmn}} = \frac{c_0}{\sqrt{\alpha_\infty}}.\end{aligned} \tag{34}$$

$$\begin{aligned}k_c(\omega \to 0) &= \omega\sqrt{\frac{\eta}{j\omega\mathcal{K}_0}\frac{\phi_{pm}}{P_0}(1+M_H)} = k_{c0\phi_p}\sqrt{\frac{\phi_{pm}}{\phi_p}(1+M_H)} = k_{c0\phi_{pm}}\sqrt{1+M_H} \\ &= k_{c0\phi_{pmn}}\sqrt{\frac{\phi_{pm}}{\phi_{pmn}}(1+M_H)}, \\ k_c(\omega \to \infty) &= \frac{\omega}{\mathcal{C}_{\infty\phi_p}} = \frac{\omega}{\mathcal{C}_{\infty\phi_{pm}}} = \frac{\omega}{\mathcal{C}_{\infty\phi_{pmn}}}.\end{aligned} \tag{35}$$

The subscripts ϕ_p, ϕ_{pm}, and ϕ_{pmn} denote the limiting values for single, double, and triple porosity non-sorptive materials respectively. These expressions show that, at low frequencies, the sound waves are both slowed down and more attenuated by a factor of $\sqrt{(\phi_{pm}/\phi_p)(1+M_H)}$, $\sqrt{1+M_H}$, and $\sqrt{(\phi_{pm}/\phi_{pmn})(1+M_H)}$ in comparison with single, double, and triple porosity non-sorptive materials, respectively. At high frequencies, the influence of sorption and the inter-scale diffusion processes vanishes.

Although not an effective parameter, it is of interest to investigate the low-frequency asymptotic behavior of the surface impedance $Z_w(\omega \to 0) = Z_{w0}$ of a rigidly-backed layer of multiscale sorptive material of thickness d_l. Provided that $|k_c(\omega)d_l| << 1$ and $\omega << \omega_{\min}$, the real and imaginary parts of the low-frequency surface impedance can be approximated by (with $\sigma_{p0} = \eta/\mathcal{K}_{p0}$ being the static flow resistivity and $\Phi = \phi_p + (1-\phi_p)(\phi_m + (1-\phi_m)H_e) = \phi_{pm}(1+M_H)$ the apparent porosity of the material):

$$\mathrm{Im}(Z_{w0}) \approx -\frac{P_0}{\omega d_l \Phi} \quad ; \quad \mathrm{Re}(Z_{w0}) \approx d_l\left(\frac{\sigma_{p0}}{3} + \frac{P_0}{\Phi^2 d_l^2 \omega_c}\right) \tag{36}$$

These equations are an important result of this paper and can serve as a basis for developing novel measurement methods of sorption and diffusion parameters of multiscale sorptive materials using sound waves. They show that the effective linearized sorption equilibrium constant H_e can be extracted from measurements of the imaginary part of the surface impedance at low frequencies, while its real part can be related to the effective diffusion coefficient D_e, provided that the other macroscopic parameters involved are known. A theoretical study assessing the feasibility of such a method has been presented in Ref. 17 for the particular case of an array of cylindrical pores embedded in a nanoporous sorptive matrix. In the present work, Eqs. (36) are developed for triple porosity sorptive materials with complex material morphology and depend on macroscopic independently measurable parameters.

The following relationships (i.e. Eq. (37)) show that the magnitude of the imaginary part of the surface impedance of a rigidly-backed layer of multiscale sorptive material is smaller than that of single, double, and triple porosity non-sorptive materials.

$$\mathrm{Im}(Z_{w0}) = \frac{\phi_p}{\phi_{pm}} \frac{\mathrm{Im}(Z_{w0\phi_p})}{1+M_H} = \frac{\mathrm{Im}(Z_{w0\phi_{pm}})}{1+M_H} = \frac{\phi_{pmn}}{\phi_{pm}} \frac{\mathrm{Im}(Z_{w0\phi_{pmn}})}{1+M_H} \tag{37}$$

The relationships between the real part of the surface impedance for sorptive and non-sorptive materials can be written as:

$$\mathrm{Re}(Z_{w0}) = \mathrm{Re}(Z_{w0\xi}) \left(1 - \frac{1 - \left(\frac{\Phi}{\Phi_\xi}\right)^2 \frac{\omega_c}{\omega_{c\xi}}}{1 + \frac{\sigma_{p0}\omega_c d_l^2 \Phi^2}{3P_0}} \right)^{-1} . \tag{38}$$

Here the subscript ξ takes values ϕ_p, ϕ_{pm}, and ϕ_{pmn} for single, double, and triple porosity non-sorptive materials. In turn, $\Phi_{\phi_p} = \Phi(\phi_m = \phi_n = 0) = \phi_p$, $\Phi_{\phi_{pm}} = \phi_{pm}$, and $\Phi_{\phi_{pmn}} = \phi_{pmn}$. The characteristic frequency takes the following values $\omega_{c\phi_p} = \omega_c(\phi_m = \phi_n = 0)$, $\omega_{c\phi_{pm}} = \omega_c(\phi_n = 0)$, and $\omega_{c\phi_{pmn}} = \omega_c(H_e = \phi_n)$. Depending on the parameters of the material, this ratio can be smaller or larger than one. This implies that the real part of the surface impedance of a sorptive material can be either smaller or larger than that of non-sorptive materials.

Finally, using Eq. (29), the sound absorption coefficient α can be written in terms of the low-frequency normalized resistance $X_0^* = (d_l/Z_0)(\sigma_{p0}/3 + P_0/(\Phi^2 d_l^2 \omega_c))$ and reactance $Y_0^* = -P_0/Z_0\omega d_l \Phi$ as:

$$\alpha(\omega \to 0) = \frac{1}{\frac{(1+X_0^*)^2}{4X_0^*} + \frac{(Y_0^*)^2}{4X_0^*}} \tag{39}$$

The denominator of this expression is minimized when its first term tends to one (i.e. $X_0^* \to 1$) and its second term is as small as possible. As Φ increases, the magnitude of the low-frequency reactance decreases. Taking into account that Φ can take values larger than one when H_e is large, the decrease in magnitude of the low-frequency reactance is much more pronounced for sorptive materials in comparison with non-sorptive ones. It then follows that sorptive materials tend to provide larger sound absorption coefficient at low frequencies. This appears as a direct consequence of the decrease of the magnitude of the low-frequency reactance, which is determined by the larger effective low-frequency dynamic compressibility caused by sorption.

IV. ANALYTICAL MODEL FOR MULTISCALE SORPTIVE GRANULAR MATERIALS

An analytical model for multiscale sorptive granular materials is introduced in this section to exemplify the theory developed in this work. A model for a packing of porous grains whose inner structure comprises two different scales of heterogeneities is considered. The hierarchical structure of the material is the same as that in Ref. 24. However, the calculation of the effective parameters associated with the nano porous domain differ. Specifically, the compressibility of the nano porous domain is calculated using a single parameter H_e, instead of three parameters; and, since the inter-scale mass diffusion is not assumed quasi-static, an analytical expression for the frequency-dependent function representing this phenomena is introduced.

The smaller inner-grain scale corresponds to the nano porous domain and is modeled as an effective medium with parameters (see Eqs. (A.6) and (A.5)): $H_e = \phi_n(\varphi+(1-\varphi)H)$ and $D_e = \phi_n(\varphi D_n + (1-\varphi)D_s H)$, where ϕ_n is the nano porosity. Taking into account that the ratio between the nanopore surface area and volume is inversely proportional to the nanopore characteristic size, the transport void fraction is approximated as $\varphi = 1 - d/r_n$, where r_n is the radius of the cylindrical nanopores. It is additionally considered that the diffusion mechanism in the bulk of the nanopores is Knudsen diffusion[1], i.e. $D_n = D_k = 2r_n v_T/3$ with v_T being the mean thermal speed; while the surface diffusion coefficient is calculated as[1]: $D_s = (1/4)\zeta v_T \exp(-E_a/R_g\tau_0)$. Here R_g is the gas constant, ζ is the distance between adjacent sites (which is approximated by the molecule size, i.e. $\zeta \approx d$), and E_a is the energy

of activation needed for a jump, which is in the order of a third of the heat of adsorption[1]. The linearized sorption equilibrium constant H can be modeled using a Langmuir isotherm model[25] (see Eq. (A.37)). Alternatively, one can directly use values of H_e and D_e as inputs to the model. It is worth noting that the former can be obtained from isotherm measurements[1], while the latter using chromatographic methods, among others[1,9,14].

The larger inner-grain scale is the micropore domain Ω_m. This is modeled as an array of cylindrical micropores with radius r_m and micro porosity ϕ_m. The dynamic viscous and thermal permeabilities associated with the micropore fluid network accounting for rarefaction effects, i.e. $\mathcal{K}_m(\omega)$ and $\Theta_m(\omega)$, are calculated from the solution of Eqs. (A.18)-(A.19) and (A.21) with boundary conditions (A.42) and (A.43), respectively. These permeabilities depend on the Knudsen number $\mathrm{Kn} = \ell/r_m$ with ℓ being the molecular mean free path, and their expressions, which involve Bessel functions $J_{0,1}$ of the first kind of order 0 and 1, have been obtained in Ref. 37 and are shown in Table I.

The pore-scale geometry is modeled as an array of spherical grains with grain radius r_p and inter-granular void porosity ϕ_p. The dynamic thermal and viscous permeabilities associated with the pore fluid network, i.e. $\Theta_p(\omega)$ and $\mathcal{K}_p(\omega)$, are calculated from the solution of Eqs. (A.18)-(A.20) and (A.21)-(A.22) (with the subscript m being replaced by p). A self-consistent approach, as detailed in Refs. 38 and 39, has been used. The expressions for these permeabilities are shown in Tables I and II, respectively.

The inter-scale (inner-grain micropores to/from nano porous domain) mass diffusion function $G(\omega)$ is obtained from the solution of Eqs. (A.23)-(A.24). A self-consistent approach, as detailed in Refs. 25 and 40, has been used. The final expression involves modified Bessel functions I_i and K_i of the first and second kind of order i and is shown in Table I.

The inter-scale (inter-granular voids to/from grains) pressure diffusion function $B(\omega)$ is calculated from the solution of Eqs. (B.4)-(B.5) using a self-consistent approach[23] and its expression is shown in table I.

TABLE I. Analytical model for the dynamic compressibility of the effective fluid saturating a multiscale sorptive granular material.

Effective dynamic compressibility $\mathsf{C}(\omega) = \mathsf{C}_p(\omega) + (1-\phi_p)\mathsf{C}_{mn}(\omega)\mathcal{F}_{pmn}(\omega),$ $\mathcal{F}_{pmn}(\omega) = 1 - \frac{j\omega B(\omega)}{(1-\phi_p)\mathcal{B}_{app}(\omega)}.$
Effective dynamic compressibility and thermal permeability of the inter-granular voids $\mathsf{C}_p(\omega) = \frac{\phi_p}{P_0}\left(1 - j\omega\rho_0 C_p \frac{\gamma-1}{\gamma}\frac{\Theta_p(\omega)}{\phi_p\kappa}\right),$ $\Theta_p(\omega) = -j(1-\beta^3)\delta_t^2\left(1 - \frac{\beta}{1-\beta^3}\frac{3}{z_t^2}\left(1 - \beta z_t \frac{1+z_t\tanh(z_t(\beta-1))}{z_t+\tanh(z_t(\beta-1))}\right)\right),$ where $\beta = \sqrt[3]{1-\phi_p}$, $\quad z_t = j^{1/2}\frac{r_p}{\beta\delta_t}$, $\quad$ and $\quad \delta_t = \sqrt{\frac{\kappa}{\rho_0 C_p \omega}}$.
Effective dynamic compressibility of the micro-nano porous domain (i.e. the grains) $\mathsf{C}_{mn}(\omega) = \mathsf{C}_m(\omega) + (1-\phi_m)\mathsf{C}_n\mathcal{F}_{mn}(\omega),$ $\mathcal{F}_{mn}(\omega) = 1 - \frac{j\omega G(\omega)}{(1-\phi_m)\mathcal{D}_{app})}.$
Effective dynamic compressibility and thermal permeability of the inner-grain micropores $\mathsf{C}_m(\omega) = \frac{\phi_m}{P_0}\left(1 - j\omega\rho_0 C_p \frac{\gamma-1}{\gamma}\frac{\Theta_m(\omega)}{\phi_m\kappa}\right),$ $\Theta_m(\omega) = -j\phi_m\delta_t^2\left(1 - \frac{2}{\mathrm{X}_t}\frac{J_1(\mathrm{X}_t)}{J_0(\mathrm{X}_t) - \mathrm{k}_t\mathrm{X}_t J_1(\mathrm{X}_t)}\right),$ with $\mathrm{X}_t = j^{3/2}\frac{r_m}{\delta_t}$, $\quad \mathrm{k}_t = 2\frac{\gamma\mathrm{Kn}}{(\gamma+1)\mathrm{Pr}}$, $\quad \mathrm{Kn} = \frac{\ell}{r_m}$, $\quad$ and $\quad \mathrm{Pr} = \frac{C_p\eta}{\kappa}$.
Effective compressibility of the inner-grain nano porous domain $\mathsf{C}_n = \frac{H_e}{P_0}.$
Inter-scale (inner-grain micropores to/from nano porous domain) mass diffusion function $G(\omega) = -j(1-\phi_m)\delta_d^2\left(1 - \frac{2\phi_m}{1-\phi_m}\frac{R_1(\xi_d)}{R_0(\xi_d)}\right),$ with $R_i(\xi_d) = \left(\frac{1}{\xi_d}\right)^i\left(K_i(\xi_d) + (-1)^i\frac{K_1(\xi_d/\sqrt{\phi_m})}{I_1(\xi_d/\sqrt{\phi_m})}I_i(\xi_d)\right), \quad i = 0, 1;$ $\xi_d = \sqrt{j}\frac{r_m}{\delta_d}$, $\quad \delta_d = \sqrt{\frac{\mathcal{D}_{app}}{\omega}}$, $\quad$ and $\quad \mathcal{D}_{app} = \frac{D_e}{H_e}.$
Inter-scale (inter-granular voids to/from grains) pressure diffusion function $B(\omega) = -j(1-\phi_p)\delta_b^2\left(1 - 3\xi_b^{-2}(1 - \xi_b\cot(\xi_b))\right),$ where $\xi_b = j^{3/2}\frac{r_p}{\delta_b}$, $\quad \delta_b = \sqrt{\frac{\mathcal{B}_{app}}{\omega}}$, $\quad$ and $\quad \mathcal{B}_{app}(\omega) = \frac{\mathcal{K}_m(\omega)}{\eta\mathsf{C}_{nm}(\omega)}.$
Viscous permeability of the inner-grain micropores $\mathcal{K}_m(\omega) = -j\phi_m\delta_v^2\left(1 - \frac{2}{\mathrm{X}_v}\frac{J_1(\mathrm{X}_v)}{J_0(\mathrm{X}_v) - \mathrm{k}_v\mathrm{X}_v J_1(\mathrm{X}_v)}\right),$ with $\mathrm{X}_v = j^{3/2}\frac{r_m}{\delta_v}$, $\quad \mathrm{k}_v = \mathrm{Kn} = \frac{\ell}{r_m}$, $\quad$ and $\quad \delta_v = \sqrt{\frac{\eta}{\rho_0\omega}}.$

TABLE II. Analytical model for the dynamic viscous permeability of a multiscale sorptive granular material.

Dynamic viscous permeability
$\mathcal{K}(\omega) = \mathcal{K}_p(\omega) = -j(1-\beta^3)\delta_v^2 \left(1 - \frac{\beta^3}{1-\beta^3} \frac{\varsigma \frac{1-\beta^3}{\beta^3}+1}{\varsigma-1}\right),$
$\varsigma = \frac{3}{z^2} \frac{A_p z + B_p \tanh(z(\beta-1))}{a_p z + b_p \tanh(z(\beta-1))},$
$A_p = (3+(\beta z)^2)\left(1+\frac{z^2}{6}\right) - 3\beta\left(1+\frac{z^2}{2}\right),$
$a_p = \frac{1}{3}(3+(\beta z)^2) - 3\beta - \frac{2}{\beta}\left(1+\frac{z^2}{6}\right) + \frac{4}{\cosh(z(\beta-1))},$
$B_p = (3+(\beta z)^2)\left(1+\frac{z^2}{2}\right) - 3\beta z^2\left(1+\frac{z^2}{6}\right),$
$b_p = 3 + \beta(\beta-1)z^2 - \frac{2}{\beta}\left(1+\frac{z^2}{2}\right),$
$\beta = \sqrt[3]{1-\phi_p}, \quad \text{and} \quad z = j^{1/2}\frac{r_p}{\beta\delta_v}.$

TABLE III. Static values of the effective dynamic permeabilities and inter-scale diffusion functions of a multiscale sorptive granular material.

$\Theta_{p0} = \frac{r_p^2}{15}\left(\frac{5-9\beta+5\beta^3-\beta^6}{\beta^3}\right)$
$\Theta_{m0} = \phi_m \frac{r_m^2}{8}\left(1 + \frac{8\gamma}{(\gamma+1)\mathrm{Pr}}\mathrm{Kn}\right)$
$G_0 = \frac{r_m^2}{8\phi_m}(-2\ln(\phi_m) + 4\phi_m - \phi_m^2 - 3)$
$B_0 = (1-\phi_p)\frac{r_p^2}{15}$
$\mathcal{K}_{m0} = \phi_m \frac{r_m^2}{8}(1+4\mathrm{Kn})$
$\mathcal{K}_{p0} = \frac{r_p^2}{3\beta^2}\left(\frac{2+3\beta^5}{\beta(3+2\beta^5)} - 1\right)$

Using the static values of the thermal permeabilities and inter-scale diffusion functions shown in table III, one can explicitly write the characteristic frequencies determining the behavior of the effective dynamic compressibility as:

$$\omega_{tp} = \frac{\phi_p \kappa}{\rho_0 C_p \Theta_{p0}} = \frac{\kappa}{\rho_0 C_p} \frac{15}{r_p^2} \frac{\beta^3(1-\beta^3)}{(5-9\beta+5\beta^3-\beta^6)}, \tag{40}$$

$$\omega_{tm} = \frac{\phi_m \kappa}{\rho_0 C_p \Theta_{m0}} = \frac{\kappa}{\rho_0 C_p} \frac{8}{r_m^2} \left(1 + \frac{8\gamma \mathrm{Kn}}{(\gamma+1)\mathrm{Pr}}\right)^{-1}, \tag{41}$$

$$\omega_d = \frac{(1-\phi_m)\mathcal{D}_{app}}{G_0} = \frac{D_e}{H_e} \frac{8}{r_m^2} \frac{\phi_m(1-\phi_m)}{(-2\ln\phi_m + 4\phi_m - \phi_m^2 - 3)}, \tag{42}$$

$$\omega_b = \frac{(1-\phi_p)\mathcal{B}_{app0}}{B_0} = \frac{P_0}{\eta} \frac{15}{8} \frac{r_m^2}{r_p^2} \phi_m \frac{1 + 4\mathrm{Kn}}{\phi_m + (1-\phi_m)H_e}. \tag{43}$$

Eq. (41) shows that rarefaction effects reduce the thermal characteristic frequency ω_{tm}, while Eq. (42) indicates that the effective mass diffusion is slowed down by sorption. This effect on the pressure diffusion characteristics of the material can, however, be compensated by rarefaction effects, as shown by Eq. (43).

The introduced model depends effectively on six parameters, namely the grain radius r_p, inter-granular porosity ϕ_p, micropore radius r_m, micro porosity ϕ_m, and the effective parameters of the nano porous domain, i.e. D_e and H_e. This model can be simplified since, for the materials of interest, the micropore size is in the order of the molecular mean free path and sound propagation in the micropores can therefore be considered as viscosity-dominated and isothermal. Hence, the dynamic viscous and thermal permeabilities associated with the micropore fluid network can be approximated, in the audible frequency range, by $\mathcal{K}_m(\omega) = \mathcal{K}_{m0}$ and $\Theta_m(\omega) = \Theta_{m0}$. This leads to $\mathsf{C}_m = \phi_m/P_0$, $\mathsf{C}_{mn} = \phi_m/P_0 + (1-\phi_m)\mathsf{C}_n\mathcal{F}_{mn}$, and $\mathcal{B}_{app} = \mathcal{K}_{m0}/\eta\mathsf{C}_{mn}$. This shows that, in the audible frequency range, sound propagation in multiscale sorptive materials is mainly affected by viscosity and heat transfer effects at the pore scale and the inter-scale mass and pressure diffusion processes. The former diffusion process is influenced by sorption while the latter by both sorption and rarefaction.

V. ILLUSTRATING EXAMPLES AND EXPERIMENTAL VALIDATION

A. Illustrating examples

The acoustical properties of multiscale sorptive porous materials are illustrated in this section. First, we present results for the effective dynamic compressibility due to its significant influence on the acoustical properties of this type of materials. We consider the following parameters of a multiscale granular sorptive material: $r_p = 1$ mm, $\phi_p = 0.4$, $r_m = 1$ μm, $\phi_m = 0.5$, $r_n = 1$ nm, $\phi_n = 0.2$, $H = 75$, and $E_a = 10$ kJ/mole. The value of the energy of activation needed for a jump E_a has been set equal to a third of the heat of

adsorption, which is in the order of 20 to 40 kJ/mole for activated carbons[1]. In addition, it should be reminded that the developed theory applies to materials saturated with a pure fluid. However, for simplicity, the saturating fluid parameters are set equal to those of air (with molecular size $d \approx 0.38$ nm), which are close to those of nitrogen at the considered normal pressure ($P_0 = 101325$ Pa) and temperature ($\tau_0 = 293.15$ K) conditions.

Figure 2 shows the real part of the effective dynamic compressibility, calculated using the model shown in table I, of a triple-porosity sorptive material normalized to the isothermal value of this quantity for a triple-porosity non-sorptive material, i.e. $\mathrm{Re}(P_0\mathsf{C}(\omega)/\phi_{pmn})$. This is compared with that of single, double, and triple porosity non-sorptive materials. Respectively, these correspond to a packing of solid grains (i.e. $\phi_n = \phi_m = 0$), and of porous grains without nanopores (i.e. $\phi_n = 0$) and with $H_e = \phi_n$ and effective diffusion coefficient $D_e = \phi_n D_k$. Sorption induces a significant increase of the real part of the dynamic compressibility at low frequencies. For the four cases, the low-frequency limiting values are well described by Eq. (33), while at high frequencies the real part of the effective dynamic compressibilities tend to the same limiting value, as predicted by Eq. (30).

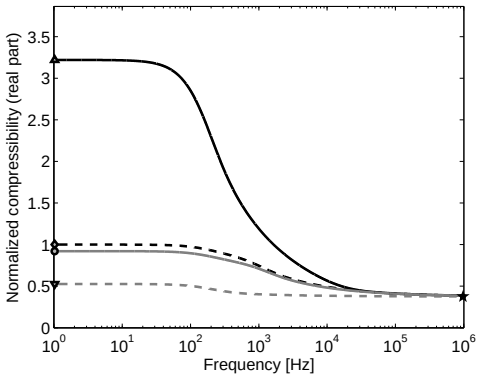

FIG. 2. Real part of the normalized effective dynamic compressibility $\mathrm{Re}(P_0\mathsf{C}(\omega)/\phi_{pmn})$ as a function of frequency. Continuous black line: multiscale sorptive granular material. Dashed black line : triple porosity non-sorptive granular material (i.e. $H_e = \phi_n$ and $D_e = \phi_n D_k$). Continuous gray line: double porosity non-sorptive granular material (i.e. $\phi_n = 0$). Dashed gray line: single porosity non-sorptive granular material (i.e. $\phi_n = \phi_m = 0$). The markers show the asymptotic values predicted by Eqs. (33) and (30).

The negative of the imaginary part of the normalized effective dynamic compressibility, which is associated with the acoustic losses in the material, and the characteristic frequencies

determining its behavior are shown in Figure 3. These have been calculated using the model shown in table I and Eqs. (32) and (40)-(43), respectively. Multiscale sorptive materials provide much larger sound attenuation than non-sorptive ones in the low frequency range. This is a direct consequence of the combined effect of heat transfer in the pores and inter-scale mass and pressure diffusion with the latter two being influenced by sorption. Such attenuation is maximized around the characteristic frequencies associated with these phenomena, i.e. around ω_{tp}, ω_d, and ω_b.

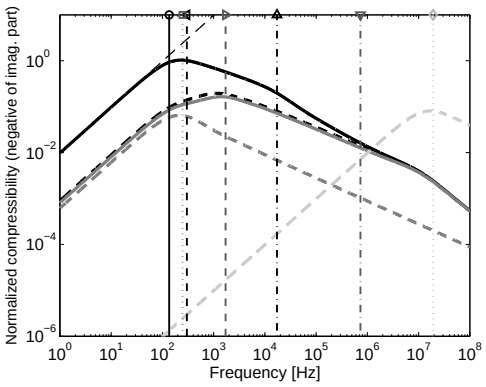

FIG. 3. Negative of the imaginary part of the normalized effective dynamic compressibility $-\mathrm{Im}(P_0\mathsf{C}(\omega)/\phi_{pmn})$ as a function of frequency. Continuous black line: multiscale sorptive granular material. Dashed black line : triple porosity non-sorptive granular material (i.e. $H_e = \phi_n$ and $D_e = \phi_n D_k$). Continuous gray line: double porosity non-sorptive granular material (i.e. $\phi_n = 0$). Dashed dark gray line: single porosity non-sorptive granular material (i.e. $\phi_n = \phi_m = 0$, non-porous grains). Dashed light gray line: single porosity non-sorptive monolithic material with micropores only (i.e. $\phi_n = \phi_p = 0$). Thin dashed black line : low-frequency asymptotic value $-\mathrm{Im}(P_0\mathsf{C}_{lf}(\omega)/\phi_{pmn})$ (see Eq. (31)). The vertical lines with markers represent characteristic frequencies. Circle : $f_c = \omega_c/2\pi$. Square: f_{tp}. Left-pointing triangle : f_b. Right-pointing triangle : f_b (no sorption). Upward-pointing triangle : f_d. Downward-pointing triangle : f_d (no sorption). Diamond : f_{tm}. The material parameters are as in Figure 2.

In comparison with a triple porosity non-sorptive material, the characteristic frequencies ω_d and ω_b decrease as a direct consequence of the local slowing down of mass diffusion by sorption (see Eq. (42)), and the increase in effective dynamic compressibility also caused by this phenomena (see Eqs. (C.3) and (43)). This can be seen by comparing the vertical lines with left-pointing and upward-pointing triangles with those with right-pointing and

downward-pointing triangles. Moreover, in the absence of sorption, the expected peak associated with inter-scale mass diffusion becomes negligible. This is because the influence of the inner-grain physics on the macroscopic behavior becomes smaller when $\omega >> \omega_b$. This indicates that in order to be able to observe (and/or take advantage of) the effects associated with the inner-grain physics, one should ideally have that $O(\omega_b) = O(\omega_d)$, i.e. $O((1-\phi_p)\mathcal{B}_{app0}B_0^{-1}) = O((1-\phi_m)\mathcal{D}_{app}G_0^{-1})$. This condition, which guarantees the rich interplay between the different physical phenomena and geometric features of multiscale sorptive materials, for the geometry considered here is given by Eq. (44) with $\mathcal{A}$ being a constant that is ideally $\mathcal{A} \geq 1$ but not extremely larger than unity.

$$\frac{64}{15}\frac{\eta}{P_0}\frac{\mathcal{D}_{app}}{r_m^2}\frac{r_p^2}{r_m^2}\frac{\phi_m + (1-\phi_m)H_e}{1+4\mathrm{Kn}}\frac{1-\phi_m}{-2\ln(\phi_m) + 4\phi_m - \phi_m^2 - 3} = \mathcal{A}. \tag{44}$$

For the material parameters considered in the example shown in Figure 3, the double porosity non-sorptive material behaves similarly as the triple-porosity non-sorptive one. The two single porosity non-sorptive materials (i.e. a packing of non-porous grain $\phi_n = \phi_m = 0$ and a monolithic material with micropores only $\phi_n = \phi_p = 0$) also displayed in Figure 3, clearly show the positions of the peaks associated with heat transfer in the pores and micropores, as well as their influence on the behavior of the multiscale material. It should be noted that, in this example, rarefaction effects are negligible since $\mathrm{Kn} = 0.06$. Hence these effects do not substantially compensate the decrease in ω_b caused by sorption. For materials with smaller micropores, rarefaction effects can become significant, as will be shown later in the paper. On the other hand, the asymptotic value of the compressibility, given by Eq. (31) and shown with thin dashed lines in Figure 3, correctly predicts the behavior for frequencies $\omega << \omega_{\min}$, while the global characteristic frequency ω_c appears as a parameter that allows identifying, in a simple manner, the frequency range where the sound attenuation is maximized. Furthermore, it should be emphasized that the results presented in Figures 2 and 3 are valid in the absence of scattering. This is estimated to occur at a frequency in the order of $f_{sca} = c_0/2\pi l_p \approx c_0/4\pi r_p$.

The effects previously discussed, i.e. inter-scale mass and pressure diffusion and sorption, lead to a decrease in sound speed and an increase of the overall sound attenuation, as predicted by Eqs. (34)-(35). This is shown in Figures 4 and 5 where the normalized speed of sound and attenuation coefficient are respectively presented. Note that i) these have been calculated using the model shown in tables I and II and Eq. (28), and ii) the normalization of

the former has been made to $c_0/\sqrt{\alpha_\infty}$ with[38] $\alpha_\infty = (3-\phi_p)/2$; while that of the attenuation coefficient to ω/c_0. In addition, the ratio of these quantities for sorptive and non-sorptive materials is well predicted by Eqs. (34) and (35), as can be seen in the inset plots.

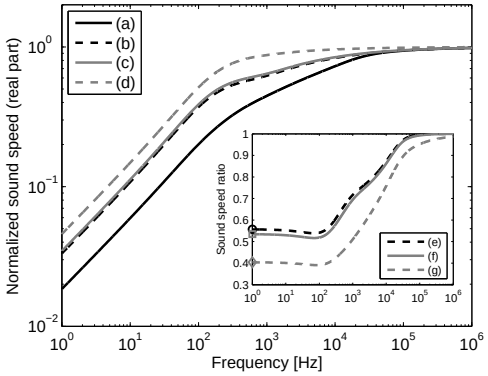

FIG. 4. Real part of the normalized sound speed $\sqrt{\alpha_\infty}\mathrm{Re}(\mathcal{C}(\omega))/c_0$ as a function of frequency for multiscale sorptive (a) and non-sorptive triple (b), double (c), and single (d) porosity granular materials. The inset plot shows the real part of the sound speed ratios: (e) $\mathrm{Re}(\mathcal{C}(\omega))/\mathrm{Re}(\mathcal{C}_{\phi_{pmn}}(\omega))$, (f) $\mathrm{Re}(\mathcal{C}(\omega))/\mathrm{Re}(\mathcal{C}_{\phi_{pm}}(\omega))$, and (g): $\mathrm{Re}(\mathcal{C}(\omega))/\mathrm{Re}(\mathcal{C}_{\phi_p}(\omega))$. The markers correspond to the low-frequency asymptotic values of these ratios (see Eq. (34)).

As discussed in Section III, the behavior in frequency of $\mathsf{C}(\omega)$ is determined by the characteristic frequencies ω_{tp}, ω_d, ω_b, and ω_{tm}, which depend on physical and geometrical parameters of the material. In particular, it has been shown in Figure 3 that the global characteristic frequency ω_c provides a good indication of the frequency range where the acoustic losses are maximized. The global characteristic frequency, calculated using Eq. (32), is shown in Figure 6 as a function of the effective diffusion coefficient D_e for different values of the effective linearized sorption equilibrium constant ($H_e = 2, 4, 8$) and micropore radii ($r_m = 0.2$ μm and $r_m = 2$ μm). The inset plot shows the characteristic frequencies f_d, f_b, and f_c as a function of D_e for $r_m = 0.2$ μm and $H_e = 4$. For a given micropore radius value, the global characteristic frequency f_c increases as D_e does until it reaches a plateau for frequencies $f_d >> f_b$. The transition is characterized by $f_d = f_b$, as shown with a vertical dotted line in the inset plot. The plateau region is reached at larger values of D_e when the micropore radius becomes larger. On the other hand, f_c decreases as H_e increases and is dominated by either f_b or f_d, whichever is much lower.

The influence of the grain radius r_p on f_c is shown in Figure 7. As previously observed,

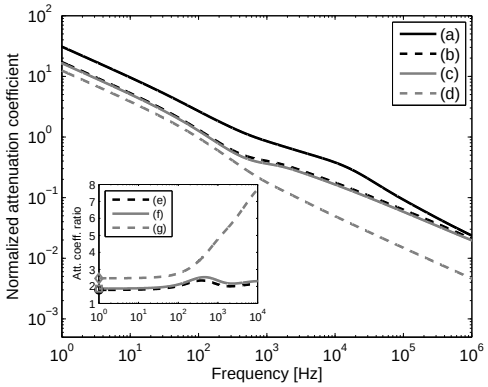

FIG. 5. Normalized attenuation coefficient $-c_0\mathrm{Im}(k_c(\omega))/\omega$ as a function of frequency for multiscale sorptive (a) and non-sorptive triple (b), double (c), and single (d) porosity granular materials. The inset plot shows the attenuation coefficient ratios : (e) $\mathrm{Im}(k_c(\omega))/\mathrm{Im}(k_{c\phi_{pmn}}(\omega))$, (f) $\mathrm{Im}(k_c(\omega))/\mathrm{Im}(k_{c\phi_{pm}}(\omega))$, and (g): $\mathrm{Im}(k_c(\omega))/\mathrm{Im}(k_{c\phi_p}(\omega))$. The markers correspond to the low-frequency asymptotic values of these ratios (see Eq. (35)).

the global characteristic frequency, calculated using Eq. (32), is dominated by f_d when $f_d << f_b$, while by f_b when $f_d >> f_b$. In addition, f_c decreases when H_e becomes larger. For small values of D_e, the influence of the grain radius on the global characteristic frequency is negligible. This is because f_c is determined by f_d, which does not depend on r_p. As D_e increases, f_c becomes larger when the grain radius is decreased. This indicates that in order to observe and/or take advantage of the sound attenuating properties of multiscale sorptive materials in the audible frequency one may prefer materials with small instead of large grains.

The influence of rarefaction effects in the modeling is now analyzed. Figure 8 shows the global characteristic frequency f_c, calculated using Eq. (32), as a function of the Knudsen number Kn for several values of micro porosity ϕ_m. Note that the results are plotted up to $\mathrm{Kn} = 1$. Although the modified continuum description is not theoretically valid for $\mathrm{Kn} > 0.1$, satisfactory agreement between measured data and theoretical predictions of rarefied gas flow through straight cylindrical tubes has been demonstrated in Ref. 37. As previously, the global characteristic frequency is determined by either f_d or f_b, whichever is much lower; as shown in the inset plot. When f_c is determined by f_b, the prediction of the global characteristic frequency is underestimated if one does not account for rarefaction effects in the modeling. As an example, f_c could be predicted to be 5 times smaller when

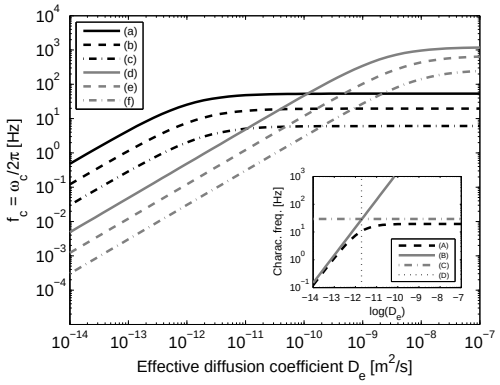

FIG. 6. Global characteristic frequency f_c as a function of the effective diffusion coefficient D_e for different values of effective linearized sorption equilibrium constant H_e and micropore radius r_m. The other parameters are as in Figure 2. Main plot : (a) $H_e = 2$ and $r_m = 0.2$ μm. (b) $H_e = 4$ and $r_m = 0.2$ μm. (c) $H_e = 8$ and $r_m = 0.2$ μm. (d) $H_e = 2$ and $r_m = 2$ μm. (e) $H_e = 4$ and $r_m = 2$ μm. (f) $H_e = 8$ and $r_m = 2$ μm. The inset plot shows the characteristic frequencies (A) f_c, (B) f_d, and (C) f_b as a function of D_e for $H_e = 4$ and $r_m = 0.2$ μm. The vertical dotted line (D) shows D_e for $f_d = f_b$.

$r_m = \ell$. Evidently, for small values of Knudsen number the influence of rarefaction effects is negligible. On the other hand, the global characteristic frequency presents higher values as the micro porosity ϕ_m increases and is maximized when the micropore radius approximately takes a value for which $O(f_d) = O(f_b)$.

Figure 9 shows the normal incidence sound absorption coefficient of a rigidly-backed 3-cm thick layer of multiscale sorptive granular material in comparison with that of non-sorptive granular ones, i.e. packing of solid grains (single porosity, $\phi_n = \phi_m = 0$), of porous grains without nanopores (double porosity, $\phi_n = 0$), and of porous grains with two inner-grain scales (triple porosity material, $H_e = \phi_n$). These have been calculated using Eqs. (29) and (28) and the model shown in tables I and II. The plot clearly shows that multiscale sorptive granular materials provide larger sound absorption coefficient than non-sorptive materials. This increase is enhanced further for larger values of H_e. The inset plot shows that α is well approximated at low frequencies by its asymptotic value Eq. (39). Hence, this provides a simple expression to evaluate the low-frequency sound absorption coefficient of multiscale sorptive materials.

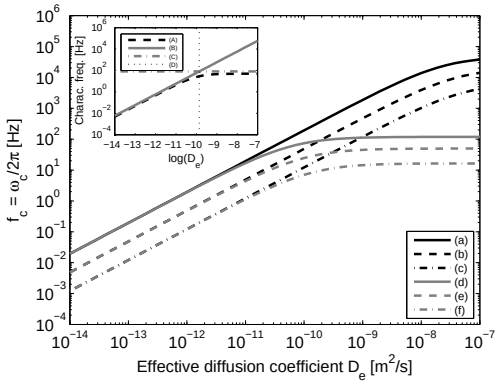

FIG. 7. Global characteristic frequency f_c as a function of the effective diffusion coefficient D_e for different values of linearized effective sorption equilibrium constant H_e and grain radius r_p. The other parameters are as in Figure 2. Main plot : (a) $H_e = 2$ and $r_p = 0.1$ mm. (b) $H_e = 4$ and $r_p = 0.1$ mm. (c) $H_e = 8$ and $r_p = 0.1$ mm. (d) $H_e = 2$ and $r_p = 2$ mm. (e) $H_e = 4$ and $r_p = 2$ mm. (f) $H_e = 8$ and $r_p = 2$ mm. The inset plot shows the characteristic frequencies (A) f_c, (B) f_d, and (C) f_b as a function of D_e for $H_e = 4$ and $r_p = 2$ mm. The vertical dotted line (D) shows D_e for $f_d = f_b$.

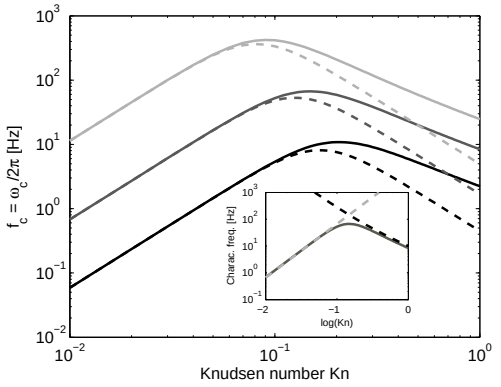

FIG. 8. Global characteristic frequency f_c as a function of the Knudsen number Kn for micro porosity values $\phi_m = 0.1$ (black lines), $\phi_m = 0.3$ (dark gray lines), and $\phi_m = 0.6$ (light gray lines). Continuous lines : model accounting for rarefaction effects. Dashed lines : model without accounting for rarefaction effects. The other parameters are $r_p = 0.75$ mm, $\phi_p = 0.3$, $D_e = 10^{-10}$ m^2/s, and $H_e = 2$. The inset plot shows f_c (continuous dark gray line), f_b (dashed black line), and f_d (dashed light gray line) as a function of Kn for $\phi_m = 0.3$.

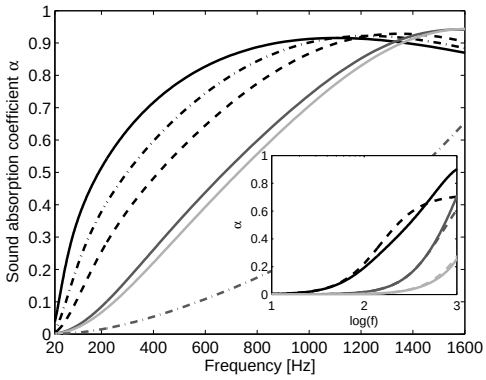

FIG. 9. Sound absorption coefficient α of a 3-cm rigidly-backed layer of material. Multiscale sorptive granular materials: black continuous ($H_e = 8$), dashed ($H_e = 4$), and dashed-dotted ($H_e = 2$) lines. Packing of non-sorptive porous grains with two inner-grain scales of heterogeneities (triple porosity, continuous dark gray line), without nano pores (double porosity, continuous light gray line), and of solid grains (single porosity, dashed-dotted gray line). Inset plot: low-frequency α for a multiscale sorptive granular material ($H_e = 4$, continuous black line), and double (continuous dark gray line) and single (continuous light gray line) porosity non-sorptive granular materials; and its asymptotic values (Eq. (39), dashed lines). The other parameters are $r_p = 0.75$ mm, $\phi_p = 0.3$, $r_m = 0.5$ μm, $\phi_m = 0.5$, $D_e = 10^{-9}$ m^2/s, and $\phi_n = 0.1$.

B. Experimental validation

1. Material characterization

This section describes the characterization of a granular activated carbon (GAC) sample. The characterization procedure for the parameters describing the inter-granular physical process and those in the micropores is similar to that in Ref. 24. The characterization of the parameters describing sorption and mass diffusion differs. Measurements of surface impedance are used to deduce these parameters, as detailed below.

The highly activated GAC sample is made out of coal, its N2 surface area is 1274 m^2/g, and its model parameters are shown in Table IV. It is detailed throughout this section how these six parameters have been measured or deduced.

An equivalent grain radius r_p of the GAC sample has been measured using optical granulometry following the procedure detailed in Refs. 22 and 23. The equivalent grain radius

TABLE IV. Parameters of the granular activated carbon sample.

ϕ_p	r_p [mm]	ϕ_m	r_m [μm]	H_e	D_e $\times 10^9$[m^2/s]
0.2997	0.7363	0.7064	0.3695	7.1189	2.9156

distribution follows a log-normal distribution $f(t|\mu,\theta) = (1/t\theta\sqrt{2\pi})\exp -(\ln t - \mu)^2/2\theta^2$ with parameters $\mu = -7.2513$ and $\theta = 0.2741$. The equivalent grain radius r_p is set to the mean value of the equivalent grain radius distribution, i.e. $r_p = 0.7363$ (0.2056) mm, where the value in round brackets corresponds to the standard deviation.

The GAC sample exhibits well separated scales. This implies that the overall permeability can be approximated by that of the pore-scale fluid network. Measurements of flow resistivity $\sigma_{p0} = \eta/\mathcal{K}_{p0}$, taken by following the procedure described in Ref. 41, are used to estimate the inter-granular void porosity ϕ_p. This is made by using the measured value of r_p and inverting the expression for $\mathcal{K}_{p0}$ shown in table III, as detailed in Ref. 23. The average flow resistivity value is $\sigma_{p0} = 24.5923$ (1.5104) kPa.s/m^2, which yields $\phi_p = 0.2997$ (0.005).

The overall porosity $\phi_{pmn} = 1 - \rho_b/\rho_C$ is calculated from the measurement of the bulk density ρ_b and the density of the material solid frame, which is assumed to be that of carbon black $\rho_C = 2.2$ g/cm^3. The measured bulk density of the GAC sample is $\rho_b = 0.335$ g/cm^3. Hence, the overall porosity is $\phi_{pmn} = 0.8477$.

The micro porosity was calculated as $\phi_m = (\phi_{pmn} - \phi_p - (1-\phi_p)\phi_n)/(1-\phi_p)(1-\phi_n)$. The nano porosity has been supplied by the manufacturer and is $\phi_n = 0.2593$. Hence, the micro porosity is $\phi_m = 0.7064$.

The effective linearized sorption equilibrium constant H_e is deduced from measurements of the imaginary part of the surface impedance $Z_w(\omega)$ of rigidly-backed layers of the GAC sample. These measurements were taken by following the procedure described in the ISO standard[42]. A vertically-installed Brüel & Kjær 4206 impedance tube was used. GAC samples with layer thickness values ranging from 2 cm to 8 cm in steps of 1 cm were measured[22,24]. The previously derived asymptotic value of the imaginary part of the surface impedance, i.e. Eq. (36), is used to determine the apparent porosity Φ. We remind that this asymptotic is valid for $|k_c d_l| << 1$ and $\omega << \omega_{min} \approx \omega_c$. A function $z_1(\omega) = \frac{P_0}{-\mathrm{Im}(Z_w)d_l} = \Phi\omega$ that is linear in frequency can be defined form Eq. (36). The apparent porosity Φ is the proportionality constant and can be obtained by linear fitting of $z_1(\omega)$. An example of this

is shown in the right-hand-side inset plot of Figure 10 for a 4-cm thick GAC sample. Then, the effective linearized sorption equilibrium constant is calculated as $H_e = ((\Phi - \phi_p)/(1 - \phi_p) - \phi_m)/(1 - \phi_m)$. Its value is $H_e = 7.1189 \pm 0.1508$.

Measurements of the real part of the surface impedance and the use of its asymptotic value allow obtaining the global characteristic frequency f_c. Using Eq. (36), a function linear in frequency $z_2(\omega) = \Phi^2 d_l^2(\mathrm{Re}(Z_w)/d_l - \sigma_{p0}/3)/P_0 = \omega/\omega_c$ can be defined. In this case, its slope is the inverse of the global characteristic frequency. Linear fitting of $z_2(\omega)$ leads to $f_c = 88.5362 \pm 5.4570$ Hz. An example of this is shown in the left-hand-side inset plot of Figure 10 for a 4-cm thick GAC sample.

The remaining parameters to be determined are r_m and D_e. The micropore radius r_m is calculated via a best-fitting routine in which the square of the absolute difference between the predicted and measured surface impedance is minimized. As part of this routine, the measured global characteristic frequency and the other parameters are used to calculate the effective diffusion coefficient D_e by inverting Eq. (32), as shown by Eq. (45). The values of the micropore radius and effective diffusion coefficient are $r_m = 0.3695$ μm and $D_e = 2.9156 \cdot 10^{-9}$ m^2/s. The values of r_m and r_p are consistent with the hypothesis of large separation of scales, i.e. $\epsilon \approx r_m/r_p = 5.0183 \times 10^{-4}$, and the estimation Eq. (A.12) holds, i.e. $\eta D_e/r_m^2 P_0 = 3.8715 \times 10^{-6} = O(\epsilon^2)$. The measured and predicted surface impedance, calculated using Eqs. (29) and (28) and the model shown in tables I and II, of a rigidly-backed 4-cm thick GAC layer is shown in the main plot of Figure 10. Note that the magnitude of the imaginary part of the surface impedance of GAC is much smaller than that of a triple porosity non-sorptive material.

$$D_e = \frac{H_e G_0}{(1-\phi_m)} \left(\frac{\frac{1}{\omega_c} - \frac{\gamma-1}{\gamma}\frac{\phi_p}{\omega_{tp}} - (1-\phi_p)\left(\frac{\gamma-1}{\gamma}\frac{\phi_m}{\omega_{tm}} + \frac{\phi_m}{\omega_b}\right)}{(1-\phi_p)(1-\phi_m)H_e} - \frac{1}{\omega_b} \right)^{-1}. \tag{45}$$

The values of r_m, D_e, and H_e compare well with those commonly found in activated carbons. For example, the size of the larger inner-grain pores, i.e. $2r_m$, is typically[1,2] in the order of 0.8 μm. Using Eq. (A.37) and considering that the nanopore size is comparable to that of the fluid molecules, the linearized sorption equilibrium constant expressed in units of adsorbed moles per mass of adsorbent is $H = 187.9$ μmol/g at normal conditions (i.e. $P_0 = 101325$ Pa and $\tau_0 = 293.15$ K). This is comparable to the data found in literature for materials saturated with nitrogen at normal pressure condition. For example, from the

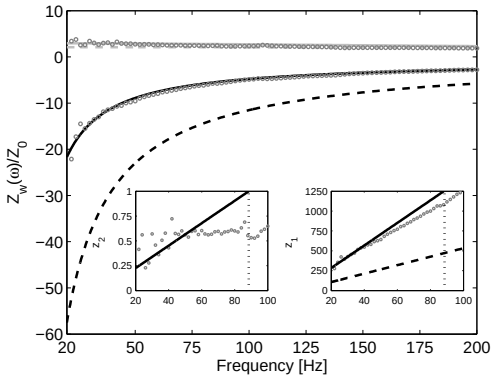

FIG. 10. Comparison between measured[22,24] (circles) and predicted real (gray lines) and imaginary (black lines) parts of the normalized surface impedance of a rigidly-backed 4-cm thick layer of granular activated carbon. Continuous lines – Triple porosity sorptive material. Dashed lines – Triple porosity non-sorptive material. The left-hand side inset plot shows $z_2(\omega)$ as a function of frequency. Circles – Measurements. Continuous line – Fitted linear function with slope $1/f_c$. The right-hand side inset plot shows $z_1(\omega)$ as a function of frequency. Circles – Measurements. Continuous line – Fitted linear function with slope Φ. Dashed line – Fitted linear function with $\Phi = \phi_{pmn}$, i.e. triple porosity non-sorptive material. In both inset plots, the dotted lines correspond to f_c

measured data in Ref. 43 for a granular activated carbon sample having a surface area of 1220 m^2/g (i.e. comparable to the GAC sample used in this paper), it is deduced that $H = 185.7$ μmol/g at 293.15 K. A value of $H = 319.9$ μmol/g is calculated from the measured data in Ref. 44 for a carbon molecular sieve 5A (i.e. a type of activated carbon) at 303.15 K. For a PCB-type activated carbon, the data in Ref. 45 leads to $H = 288.3$ μmol/g (at 293.15 K), while for a carbon molecular sieve in pellet form a value of $H = 175.8$ μmol/g (at 300.15 K) is calculated from the data in Ref. 46.

The values of D_e and H_e lead to an apparent mass diffusivity of $\mathcal{D}_{app} = 4.1 \cdot 10^{-10}$ m^2/s. For the case of nanopore pore size comparable to that of the fluid molecules, $\mathcal{D}_{app}$ can be interpreted as an activated diffusivity. Chromatographic measurements of this parameter have been reported in Ref. 47 for carbon molecular sieve 5A saturated with nitrogen. Its value at 293.15 K is $\mathcal{D}_{app} = 1.85 \cdot 10^{-11}$ m^2/s. For the same type of material and saturating fluid, measurements reported in Ref. 44 using a gravimetric technique provides $\mathcal{D}_{app} = 1.19 \cdot 10^{-10}$ m^2/s at 303 K. In Ref. 48 measurements on an activated carbon

monolith saturated with nitrogen provided a value of $\mathcal{D}_{app} = 1.35 \cdot 10^{-10}$ m^2/s at 293.15 K. Furthermore, values of $\mathcal{D}_{app} = 1.93 \cdot 10^{-9}$ m^2/s and $\mathcal{D}_{app} = 7.4 \cdot 10^{-10}$ m^2/s at 296 K have been reported in Ref. 49 for two different activated carbon monoliths saturated with nitrogen.

2. Measurements and predictions of sound absorption coefficient

Figure 11 compares measured[22,24] and predicted normal incidence sound absorption coefficient of a rigidly-backed 3-cm thick layer of granular activated carbon. The model, given by Eqs. (29), (28), and those in tables I and II, accurately predicts the measured data. Its predictions for non-sorptive materials are also plotted to highlight the absorptive properties of granular activated carbon. It is clearly observed that a sorptive material shows remarkably higher sound absorption coefficient values at low frequencies in comparison with non-sorptive ones, regardless of whether these feature multiple scales of heterogeneities. The absorption of sound is primarily caused by the combined influence of viscosity and heat transfer effects at the pore scale and the inter-scale mass and pressure diffusion processes, being the former one influenced by sorption while the latter by both sorption and rarefaction.

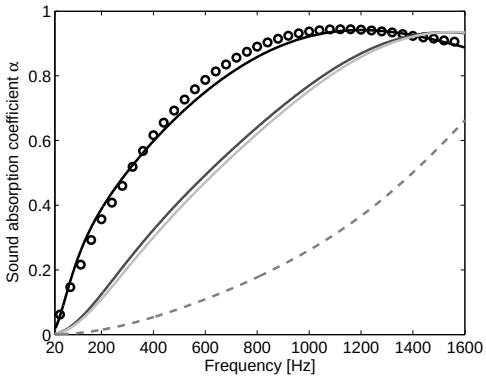

FIG. 11. Normal incidence sound absorption coefficient of a rigidly-backed 3-cm thick layer of granular activated carbon. Measurements[22,24] (circles) versus predictions for triple porosity sorptive material (black line) and triple (dark gray line), double (light gray line), and single (dashed gray line) porosity non-soprtive materials.

VI. CONCLUSIONS

This paper investigated sound propagation in multiscale rigid-frame porous materials accounting for the effects of viscosity and heat transfer at the pore scale, viscosity and heat transfer including rarefaction effects at the micropore scale, inter-scale (pore to/from micro-nanopore scales) pressure diffusion, inter-scale (micropore to/from nanopore scales) mass diffusion, and sorption in the nanopores. The two-scale asymptotic method of homogenization for periodic media has been successively used to derive the macroscopic equations describing sound propagation through the material. These show that, at the leading order, the physical processes in the micro-nano porous domain do not modify the macroscopic fluid flow, provided that the advective mass flux pulsed from the micropores on the pore boundaries is of one order smaller than the advective mass flux generated by the incident wave in the pores. As a consequence, the dynamic Darcy's law and the dynamic viscous permeability correspond to those of single porosity non-sorptive materials. Contrarily, the dynamic compressibility of the effective saturating fluid is significantly altered by the physical processes occurring at the micro- and nano scales.

We have demonstrated that sorption effects occurring in pores of nanometer size still significantly modify the macroscopic mass balance. This modification is accounted for by the dynamic compressibility of the effective saturating fluid which presents atypical properties that lead to a slower speed of sound and higher sound attenuation in the material. The strength of these macroscopic effects in the audible frequency range largely depends on the geometry and pressure and mass diffusion properties of the material. For example, relatively fast diffusing gas-solid systems whose pressure diffusion behavior is determined by a characteristic frequency that is in the order of that characterizing mass diffusion may be preferred over either slow mass diffusing systems or materials featuring slow pressure diffusion.

Contrarily to sorption effects, we have shown that rarefied gas flow in pores with size comparable to the molecular mean free path only intervene in the macroscopic acoustic behavior indirectly via a modification of the apparent pressure diffusivity.

The derived low-frequency asymptotics of the surface impedance, which is a quantity commonly measured in the field of acoustics of porous media, were used in conjunction with a characterization procedure to deduce the effective linearized sorption equilibrium constant

and effective diffusion coefficient of granular activated carbon. This provides empirical evidence supporting an alternative acoustic method for measuring sorption and mass diffusion properties of multiscale sorptive materials.

The developed theory was then validated experimentally by comparing its predictions with sound absorption measurements on a granular activated carbon sample showing good agreement.

In addition to the direct applications of the results presented in this paper to acoustics, one can consider applications to chemical engineering metrology and geophysics. Extensions of this work may include the study of sound propagation in multiscale sorptive porous materials saturated with fluid mixtures as well as the inclusion of the elasticity of the solid frame into the modeling.

ACKNOWLEDGMENTS

This work was supported by the project METAUDIBLE, co-funded by the Agence Nationale de la Recherche ANR (ANR 13-BS09-0003-03) and Fondation de Recherche pour l'Aéronautique et l'Espace FRAE, and has been conducted within the framework of CeLyA of Université de Lyon operated by ANR (ANR 10 Labex 0060- ANR 11 IDEX - 0007). We also acknowledge support from the European Union Cost Action C15125 "Designs for Noise Reducing Materials and Structures (DENORMS)" which facilitated discussion on this topic.

Appendix A

This appendix provides the derivation of the upscaled model for sound propagation in the micro-nano porous domain. First we recall the model for double porosity sorptive materials developed in Ref. 25. This is then extended to account for rarefaction effects at the micropore scale.

1. Governing equations

The governing equations for diffusion and sorption of a pure fluid in the nano porous domain are formulated first. In doing so, it is assumed that[1,25]: i) sorption occurs on the walls of the nanopores, ii) the adsorbed molecules (adsorbate) and the gas phase molecules

saturating the nanopores are in "dynamic instantaneous" equilibrium, and iii) the fluid molecules are diffused through the nano porous domain via two diffusion mechanisms, i.e. diffusion in the bulk of the nanopores and surface diffusion on the nanopore walls.

Since the characteristic sizes associated with the micro and nano scales are well separated, i.e. $l_n/l_m << 1$, the nano porous domain is modeled as an equivalent continuum governed by effective equations defined in Ω_n and reflect the local physical processes. For simplicity, it is assumed that the nano porous domain is isotropic. The constitutive flux equation accounting for the two mentioned diffusion mechanisms is given by[1,25]:

$$J = -\phi_n(\varphi D_n \nabla c_n + (1-\varphi) D_s \nabla c_s), \tag{A.1}$$

where J is the molar mass flux, c_n and c_s are, respectively, the concentration of the gas (in mole/volume of fluid) and adsorbed (in mole/volume of adsorbed phase) phases, D_n is the nanopore diffusion coefficient, and D_s is the surface diffusion coefficient. The transport void fraction $\varphi = \Omega_v/\Omega_{nf}$ represents the fraction of the nano porous void space available for the transport of free molecules. Similarly, $(1-\varphi) = \Omega_s/\Omega_{nf}$ represents the fraction of space available for the transport of adsorbed molecules (see Figure 1).

Performing a mass balance in a volume element of the nano porous domain leads to the following equation[1,25] :

$$j\omega\phi_n(\varphi c_n + (1-\varphi)c_s) = \phi_n \nabla \cdot (\varphi D_n \nabla c_n + (1-\varphi) D_s \nabla c_s) \quad \text{in} \quad \Omega_n. \tag{A.2}$$

As mentioned above, the adsorbed phase is assumed to be in "dynamic instantaneous" equilibrium with the gas phase. This is valid when the local adsorption kinetics is much faster than the diffusion processes. Such a situation is commonly found in nano porous media and is justified by the fact that the average residence time of adsorption ranges from 10^{-13} to 10^{-9} s for physical adsorption[1]. The equilibrium relationship between the two phases is then given by:

$$c_s = H c_n \quad \text{in} \quad \Omega_n, \tag{A.3}$$

where H is the linearized sorption equilibrium constant and is associated with the slope of the local isotherm at a given equilibrium point, as shown for a Langmuir isotherm model further below.

Replacing Eq. (A.3) into Eq. (A.2) and writing the concentration in terms of density,

i.e. $\rho_n = c_n M$, where M is the molar mass of the gas, lead to the Fickian equation[1,5,25]:

$$j\omega\rho_n H_e = D_e \nabla \cdot \nabla \rho_n \quad \text{in} \quad \Omega_n, \tag{A.4}$$

where the effective diffusion coefficient D_e and the effective linearized sorption equilibrium constant H_e are given by:

$$D_e = \phi_n(\varphi D_n + (1-\varphi) D_s H), \tag{A.5}$$

$$H_e = \phi_n(\varphi + (1-\varphi) H). \tag{A.6}$$

The equations of fluid motion in the micropores comprise the linearized equations of conservation of momentum, mass, and energy, and equation of state. These are respectively given by Eqs. (1), (2), (3), and (4) with the subscript p being replaced by m and are coupled with Eq. (A.4) via the following boundary conditions expressing the continuity of normal mass flux and pressure, and of negligible temperature variations and tangential mass flux on the micropore boundary Γ_m.

$$\rho_0 \mathbf{u}_m \cdot \mathbf{n}_m = -D_e \nabla \rho_n \cdot \mathbf{n}_m \quad \text{on} \quad \Gamma_m, \tag{A.7}$$

$$\rho_0(\mathbf{u}_m - (\mathbf{u}_m \cdot \mathbf{n}_m)\mathbf{n}_m) = \mathbf{0} \quad \text{on} \quad \Gamma_m, \tag{A.8}$$

$$p_n = p_m \quad \text{i.e.} \quad \rho_n = \frac{\rho_0}{P_0} p_m \quad \text{on} \quad \Gamma_m, \tag{A.9}$$

$$\tau_m = 0 \quad \text{on} \quad \Gamma_m. \tag{A.10}$$

Here the density and pressure in the effective nano porous domain are represented by ρ_n and p_n. The oscillatory fluid velocity, pressure, and temperature in the micropores are respectively denoted as $\mathbf{u}_m$, p_m, and τ_m. The outward-pointing normal vector is $\mathbf{n}_m$ (see Figure 1).

2. Homogenization procedure

The homogenization procedure described in Section II C is then applied. Now we consider the small parameter $\varepsilon = l_m/l_p << 1$ and that the fast spatial variable y is associated with fluctuations at the micropore (local) scale while the slow spatial variable x with variations at the pore (larger) scale. The rescaled set of governing equations is formulated by assessing whether the variables fluctuate at the local or larger scale, as well as by considering the relative order of magnitude of the different terms in the governing equations. The oscillatory

fluid velocity $\mathbf{u}_m$, temperature τ_m, and density ρ_n vary at the local scale, while the pressure p_m at the larger scale[25]. The relative order of magnitude of the different terms in the equations of conservation of momentum, mass, and energy, and of state associated with the micropore fluid network are the same as those discussed in Section II C. On the other hand, the most general regime of mass diffusion/sorption occurs when both terms in Eq. (A.4) are of the same order of magnitude, i.e. $O(D_e\rho_n/l_m^2) = O(\omega\rho_n H_e)$. In addition, the long-wavelength condition imposes that, on the micropore boundary Γ_m, the diffusive mass flux is of one order smaller than the advective mass flux in the micropores[25], i.e.

$$\mathcal{J} = \frac{|D_e\nabla\rho_n|}{|\rho_0\mathbf{u}_m|} = O(\varepsilon). \tag{A.11}$$

This can be written in terms of physical parameters as[25]:

$$\mathcal{J} = O\left(\frac{\rho_n}{u_m}\frac{D_e}{l_m\rho_0}\right) = O\left(\frac{\eta D_e}{P_0}\frac{l_p}{l_m^3}\right) = O(\varepsilon), \quad \text{i.e.} \quad \frac{\eta D_e}{l_m^2 P_0} = O(\varepsilon^2), \tag{A.12}$$

and indicates that the effective description of sound propagation in the micro-nano porous domain to be derived is valid when the combination of physical parameters P_0, η, D_e, and l_m satisfies the estimation Eq. (A.12).

The rescaled set of equations is then given by Eqs. (12), (13), and (14) with the subscript p being replaced by m, Eq. (A.13), and boundary conditions (A.14)-(A.17).

$$\varepsilon^2 D_e\nabla\cdot\nabla\rho_n = j\omega\rho_n H_e \quad \text{in} \quad \Omega_n. \tag{A.13}$$

$$\rho_0\mathbf{u}_m\cdot\mathbf{n}_m = -\varepsilon^2 D_e\nabla\rho_n\cdot\mathbf{n}_m \quad \text{on} \quad \Gamma_m, \tag{A.14}$$

$$\rho_0(\mathbf{u}_m - (\mathbf{u}_m\cdot\mathbf{n}_m)\mathbf{n}_m) = \mathbf{0} \quad \text{on} \quad \Gamma_m, \tag{A.15}$$

$$\rho_n = \frac{\rho_0}{P_0}p_m \quad \text{on} \quad \Gamma_m, \tag{A.16}$$

$$\tau_m = 0 \quad \text{on} \quad \Gamma_m. \tag{A.17}$$

Note that the ε^2-rescaling in the boundary condition (A.14) results from (i) the physical estimate (A.11) stating that the diffusive flux is of one order smaller than the advective one, and (ii) the fact that ρ_n varies at the local scale.

The physical variables are then looked for in the form of asymptotic expansions in powers of the small parameter $\varepsilon = l_m/l_p$ as $Q(x,y) = \sum_{i=0}^{\infty}\varepsilon^i Q^{(i)}(x,y)$ where $Q = p_m, \mathbf{u}_m, \tau_m, \rho_n$. These are then substituted into the rescaled set of equations and the terms of the same order are identified. At ε^{-1} it follows from the equation of conservation of momentum that

$\nabla_y p_m^{(0)} = 0$, which means that the pressure varies at the larger scale, i.e. $p_m^{(0)} = p_m^{(0)}(x)$. Further identification provides the following leading-order cell problems.

Fluid flow:

$$\eta \nabla_y^2 \mathbf{u}_m^{(0)} - \nabla_y p_m^{(1)} = j\omega\rho_0 \mathbf{u}_m^{(0)} + \nabla_x p_m^{(0)} \quad \text{in} \quad \Omega_{mf}, \tag{A.18}$$

$$\nabla_y \cdot \mathbf{u}_m^{(0)} = 0 \quad \text{in} \quad \Omega_{mf}, \tag{A.19}$$

$$\mathbf{u}_m^{(0)} = \mathbf{0} \quad \text{on} \quad \Gamma_m. \tag{A.20}$$

Heat conduction:

$$\kappa \nabla_y \cdot \nabla_y \tau_m^{(0)} = j\omega C_p \rho_0 \tau_m^{(0)} - j\omega p_m^{(0)} \quad \text{in} \quad \Omega_{mf}, \tag{A.21}$$

$$\tau_m^{(0)} = 0 \quad \text{on} \quad \Gamma_m. \tag{A.22}$$

Mass diffusion:

$$D_e \nabla_y \cdot \nabla_y \rho_n^{(0)} = j\omega \rho_n^{(0)} H_e \quad \text{in} \quad \Omega_n, \tag{A.23}$$

$$\rho_n^{(0)} = \frac{\rho_0}{P_0} p_m^{(0)} \quad \text{on} \quad \Gamma_m. \tag{A.24}$$

The solutions of the fluid flow (i.e. Eqs. (A.18)-(A.20)) and heat conduction (i.e. Eqs. (A.21)-(A.22)) problems are given by[29,30,32]:

$$\mathbf{u}_m^{(0)} = -\frac{\bar{\mathbf{k}}_m(y,\omega)}{\eta} \cdot \nabla_x p_m^{(0)}, \tag{A.25}$$

$$p_m^{(1)} = -\bar{\pi}_m(y,\omega) \cdot \nabla_x p_m^{(0)} + \bar{p}_m^{(1)}(x), \tag{A.26}$$

$$\tau_m^{(0)} = \frac{\bar{\theta}_m(y,\omega)}{\kappa} j\omega p_m^{(0)}, \tag{A.27}$$

where $\bar{\mathbf{k}}_m(y,\omega)$ and $\bar{\theta}_m(y,\omega)$ represent the $\Omega_m -$ periodic local fields of velocity and temperature respectively. The pressure field has been expressed in terms of its zero mean part $\bar{\pi}_m(y,\omega)$ and an integration constant $\bar{p}_m^{(1)}(x)$.

The solution of the mass diffusion problem (i.e. Eqs.(A.23) and (A.24)) is given by[6,25]:

$$\frac{\rho_n^{(0)}}{\rho_0} = \frac{p_m^{(0)}}{P_0} \left(1 - \frac{j\omega \bar{g}(y,\omega)}{\mathcal{D}_{app}}\right), \tag{A.28}$$

where $\bar{g}(y,\omega)$ represents the $\Omega_m -$ periodic local diffusive density field and the apparent diffusivity $\mathcal{D}_{app}$ is defined as:

$$\mathcal{D}_{app} = \frac{D_e}{H_e} = \frac{\varphi D_n + (1-\varphi) D_s H}{\varphi + (1-\varphi) H}. \tag{A.29}$$

3. Effective model for sound propagation in the micro-nano porous domain

The leading-order mass balance equation, i.e. Eq. (13) with the subscript p being replaced by m, integrated over the micropore space Ω_{mf} and divided by the volume Ω_m is given by:

$$j\omega \left\langle \frac{p_m^{(0)}}{P_0} - \frac{\tau_m^{(0)}}{\tau_0} \right\rangle_m + \langle \nabla_x \cdot \mathbf{u}_m^{(0)} \rangle_m + \langle \nabla_y \cdot \mathbf{u}_m^{(1)} \rangle_m = 0, \tag{A.30}$$

where the averaging operator is defined as:

$$\langle \cdot \rangle_m = \frac{1}{\Omega_m} \int_{\Omega_{mf}} \cdot \, d\Omega. \tag{A.31}$$

The term $\langle \nabla_y \cdot \mathbf{u}_m^{(1)} \rangle_m$ in Eq. (A.30) is calculated by making successive use of the divergence theorem, noting that the surface integrals on opposite boundaries of the cell cancel out due to periodicity, and using the boundary condition (A.14) identified at ε^1 (i.e. $\rho_0 \mathbf{u}_m^{(1)} \cdot \mathbf{n}_m = -D_e \nabla_y \rho_n^{(0)} \cdot \mathbf{n}_m$ on Γ_m) and Eqs. (A.23) and (A.28). Its expression is:

$$\langle \nabla_y \cdot \mathbf{u}_m^{(1)} \rangle_m = j\omega p_m^{(0)} \frac{H_e}{P_0} \frac{1}{\Omega_m} \int_{\Omega_n} \left(1 - \frac{j\omega \bar{g}(y,\omega)}{\mathcal{D}_{app}} \right) d\Omega. \tag{A.32}$$

The effective model for sound propagation in the micro-nano porous domain is then obtained by i) replacing Eq. (A.32) into Eq. (A.30), ii) substituting $\tau_m^{(0)}$ (i.e. Eq. (A.27)) and $\rho_n^{(0)}$ (i.e. Eq. A.28) in Eq. (A.30), iii) using the thermodynamic identity $P_0/\tau_0 = \rho_0 C_p(\gamma - 1)/\gamma$ (where γ is the specific heat ratio), and iv) considering that the averaged velocity is determined from Eq. (A.25). The mass balance equation and constitutive fluid flow law are given by:

$$\nabla \cdot \mathbf{U}_m + j\omega p_m \mathsf{C}_{mn} = 0, \tag{A.33}$$

$$\mathbf{U}_m = -\frac{\mathbf{k}_m(\omega)}{\eta} \cdot \nabla p_m. \tag{A.34}$$

Here the Darcy's velocity is given by $\mathbf{U}_m = \langle \mathbf{u}_m^{(0)} \rangle_m$ and since the derivatives are taken with respect to the larger-scale spatial variable and the pressure and Darcy's velocity are leading order terms, we have dropped the superscript $^{(0)}$ and the index x here and in the main text. The dynamic viscous permeability associated with the micropore fluid network is calculated as $\mathbf{k}_m(\omega) = \langle \bar{\mathbf{k}}_m(y,\omega) \rangle_m$. The effective dynamic compressibility $\mathsf{C}_{mn}(\omega)$ is given by Eq. (25), i.e. $\mathsf{C}_{mn} = \mathsf{C}_m + (1 - \phi_m)\mathsf{C}_n \mathcal{F}_{mn}$, and corresponds to the sum of the classical effective dynamic compressibility accounting for heat transfer in the micropores $\mathsf{C}_m(\omega)$, and an additional effective dynamic compressibility C_n that accounts for sorption in

the nanopores and is modified by the inter-scale mass diffusion. The latter is also affected by sorption and is accounted for by $\mathcal{F}_{mn}(\omega)$. The compressibility C_m is calculated using Eq. (23) with the subscript p being replaced by m and the associated dynamic thermal permeability is calculated as $\Theta_m(\omega) = \langle \bar{\theta}_m(y,\omega) \rangle_m$. The compressibility C_n is given by Eq. (26) and $\mathcal{F}_{mn}$ is related to the inter-scale (micro-nano) mass diffusion function $G(\omega)$ via Eq. (27). The latter is calculated as[25]:

$$G(\omega) = \frac{1}{\Omega_m} \int_{\Omega_n} \bar{g}(y,\omega) d\Omega. \tag{A.35}$$

In summary, the effective model for sound propagation in the micro-nano porous domain, given by Eqs. (A.33) and (A.34), allows concluding that the constitutive fluid flow law of the micropore fluid network and the dynamic viscous permeability are not modified by the inter-scale mass diffusion and sorption in the nanopores. Conversely, the effective dynamic compressibility becomes significantly modified by inter-scale mass diffusion and sorption. This modification comes from the appearance of a source term in the mass balance equation (i.e. the third term in Eq. (A.30)) that accounts for the contribution of both processes.

As shown in Section III, the low-frequency behavior of the effective dynamic compressibility is determined by H_e, which depends on H. A linearized dynamic sorption model derived in Ref. 25 allows linking H with the parameters of the classical Langmuir kinetics model[34]. Its use leads to replace Eq. (A.3) by $c_s = \mathcal{H}(\omega) c_n$, where the linearized sorption "dynamic equilibrium" constant is given by:

$$\mathcal{H}(\omega) = \frac{\rho_N}{\rho_0} \frac{bP_0}{(1+bP_0)^2} \frac{1}{(1+\frac{j\omega}{\omega_a})}. \tag{A.36}$$

Here $\omega_a = k_a P_0 + k_d$ is the sorption characteristic frequency, k_a is the adsorption constant (in 1/Pa/s), k_d is the desorption constant (in 1/s), and $b = k_a/k_d$ is the Langmuir constant (in 1/Pa), and ρ_N is the maximum density increment due to sorption. Since the average residence time of adsorption, i.e. $\tau_a = 1/\omega_a$, ranges from 10^{-13} to 10^{-9} s for physical adsorption[1], the sorption characteristic frequency takes very high values and $\mathcal{H}(\omega)$ can be approximated by[25]:

$$H = \mathcal{H}(\omega << \omega_a) = \frac{\rho_N}{\rho_0} \frac{bP_0}{(1+bP_0)^2}. \tag{A.37}$$

4. Rarefaction effects on sound propagation in the micro-nano porous domain

For micropores with sizes comparable to the molecular mean free path $\ell = \frac{\eta}{P_0}\sqrt{\pi R_g \tau_0/2M}$ with R_g being the gas constant, effects related to the molecular nature of the gas start becoming considerable[37,40,50–53]. The ratio between ℓ and the micropore characteristic size, known as the Knudsen number $\mathrm{Kn} = \ell/l_m$, measures the degree of rarefaction. Its value is used for assessing the validity of the continuum hypothesis[50]. For $\mathrm{Kn} < 0.01$, this hypothesis remains valid and the set of equations discussed in Section A 1 holds. For $0.01 < \mathrm{Kn} < 0.01$ (commonly referred to as the slip-flow regime), the continuum description is valid everywhere in the micropore fluid network except in a thin Knudsen layer close to the micropore walls. In order to account for this effect, the continuum description is modified by allowing a degree of tangential-velocity slip[51]. Hence the boundary conditions (A.7) and (A.8) are replaced by Eq. (A.38). Similarly, molecular effects influence the thermal behavior of materials with $l_m = O(\ell)$. For $0.01 < \mathrm{Kn} < 0.1$, the continuum description is modified to account for the temperature-jump on the micropore boundaries. This is achieved by replacing Eq.(A.10) by the so-called temperature-jump boundary condition Eq. (A.39), which states that the temperature is proportional to the normal component of the temperature gradient[37,40,52]. In these equations, $\mathbf{t}_m$ is the tangential vector collinear with the velocity slip and the velocity slip and temperature jump coefficients are respectively denoted by c_v and c_t and are assumed equal to one, i.e. the molecules are reflected diffusively[50].

$$\mathbf{u}_m = \left(-\frac{D_e}{\rho_0}\nabla\rho_n \cdot \mathbf{n}_m\right)\mathbf{n}_m - c_v\ell(\mathbf{t}_m \cdot \nabla\mathbf{u}_m \cdot \mathbf{n}_m)\mathbf{t}_m \quad \text{on} \quad \Gamma_m, \tag{A.38}$$

$$\tau_m = c_t\frac{2\gamma}{\gamma+1}\mathrm{Pr}\ell\nabla\tau_m \cdot \mathbf{n}_m \quad \text{on} \quad \Gamma_m. \tag{A.39}$$

Reminding that the velocity $\mathbf{u}_m$, temperature τ_m, and density ρ_n vary at the local scale, and using Eq. (A.11); these boundary conditions rewritten in rescaled form are given by:

$$\mathbf{u}_m = \left(-\varepsilon^2\frac{D_e}{\rho_0}\nabla\rho_n \cdot \mathbf{n}_m\right)\mathbf{n}_m - \varepsilon\ell(\mathbf{t}_m \cdot \nabla\mathbf{u}_m \cdot \mathbf{n}_m)\mathbf{t}_m \quad \text{on} \quad \Gamma_m, \tag{A.40}$$

$$\tau_m = \varepsilon\frac{2\gamma}{\gamma+1}\mathrm{Pr}\ell\nabla\tau_m \cdot \mathbf{n}_m \quad \text{on} \quad \Gamma_m. \tag{A.41}$$

The application of the homogenization procedure leads to the fluid flow and heat conduction leading-order cell problems Eqs. (A.18)-(A.19) and (A.21) with the boundary conditions (A.20) and (A.22) being respectively replaced by :

$$\mathbf{u}_m^0 = -\ell(\mathbf{t}_m^{(0)} \cdot \nabla_y\mathbf{u}_m^{(0)} \cdot \mathbf{n}_m)\mathbf{t}_m^{(0)} \quad \text{on} \quad \Gamma_m, \tag{A.42}$$

$$\tau_m^{(0)} = \frac{2\gamma}{\gamma+1}\mathrm{Pr}\ell\nabla_y\tau_m^{(0)}\cdot\mathbf{n}_m \quad \text{on} \quad \Gamma_m. \tag{A.43}$$

These resulting leading-order cell problems have been solved in Refs. 22, 24, and 53. Their solutions, which are given by Eqs. (A.44) and (A.45), replace Eqs. (A.25) and (A.27).

$$\mathbf{u}_m^{(0)} = -\frac{\bar{\mathbf{k}}_m(y,\omega,\mathrm{Kn})}{\eta}\cdot\nabla_x p_m^{(0)}, \tag{A.44}$$

$$\tau_m^{(0)} = \frac{\bar{\theta}_m(y,\omega,\mathrm{Kn})}{\kappa} j\omega p_m^{(0)}. \tag{A.45}$$

Further algebra leads to the effective model for sound propagation in the micro-nano porous domain given by Eqs. (20)-(21). However, its effective parameters are modified by rarefaction effects. Specifically, the dynamic viscous and thermal permeabilities associated with the micropore fluid network are calculated as $\mathbf{k}_m(\omega,\mathrm{Kn}) = \langle\bar{\mathbf{k}}_m(y,\omega,\mathrm{Kn})\rangle_m$ and $\Theta_m(\omega,\mathrm{Kn}) = \langle\bar{\theta}_m(y,\omega,\mathrm{Kn})\rangle_m$. Consequently, the effective dynamic compressibilities C_m and C_{mn} are also affected by rarefaction effects.

It then follows that sound propagation in multiscale sorptive materials is affected by rarefaction effects via the dependence of the effective dynamic compressibility C on both C_{mn} and $\mathcal{F}_{pmn}$. In particular, the modification by rarefaction effects of the latter comes from their influence on the pressure field $p_m^{(0)}$ in Eq. (B.6), which is determined by the apparent pressure diffusivity (i.e. Eq. (B.7)) that becomes Knudsen number-dependent, i.e. $\mathcal{B}_{app}(\omega,\mathrm{Kn}) = \mathcal{K}_m(\omega,\mathrm{Kn})/\eta\mathsf{C}_{mn}(\omega,\mathrm{Kn})$.

Appendix B

This appendix provides the mathematical details of the derivation of the macroscopic equations (20) and (21) that describe sound propagation in multiscale sorptive materials.

Replacing the variables written as asymptotic expansions in powers of the small parameter ϵ, i.e. $Q(x,y) = \sum_{i=0}^{\infty}\epsilon^i Q^{(i)}(x,y)$ where $Q = p_p, \mathbf{u}_p, \tau_p, \rho_p, p_m, \mathbf{U}_m$, into Eqs. (12)-(19) and identifying the terms of the same order lead to the following results. At ϵ^{-1}, it follows from the equation of conservation of momentum that $\nabla_y p_p^{(0)} = 0$, which implies that the pore pressure is a macroscopic variable, i.e. $p_p^{(0)} = p_p^{(0)}(x)$. Further identification leads to the oscillatory Stokes and heat conduction problems in the pore fluid network. These are respectively given by Eqs. (A.18)-(A.20) and (A.21)-(A.22) with the subscript m being

replaced by p. Their solutions are given by[29,30,32]:

$$\mathbf{u}_p^{(0)} = -\frac{\bar{\mathbf{k}}_p(y,\omega)}{\eta} \cdot \nabla_x p_p^{(0)}, \tag{B.1}$$

$$p_p^{(1)} = -\bar{\pi}_p(y,\omega) \cdot \nabla_x p_p^{(0)} + \bar{p}_p^{(1)}(x), \tag{B.2}$$

$$\tau_p^{(0)} = \frac{\bar{\theta}_p(y,\omega)}{\kappa} j\omega p_p^{(0)}. \tag{B.3}$$

where $\bar{\mathbf{k}}_p(y,\omega)$ and $\bar{\theta}_p(y,\omega)$ represent the Ω_p-periodic local fields of velocity and temperature respectively. The pressure field has been expressed in terms of its zero mean part $\bar{\pi}_p(y,\omega)$ and an integration constant $\bar{p}_p^{(1)}(x)$.

In the micro-nano porous domain, which is assumed isotropic for simplicity, the local pressure field is imposed by the pore pressure on Γ_p and is governed by the following set of equations:

$$\nabla_y \cdot \left(-\frac{\mathcal{K}_m}{\eta} \nabla_y p_m^{(0)} \right) + j\omega p_m^{(0)} \mathsf{C}_{mn} = 0 \quad \text{in} \quad \Omega_{mn}, \tag{B.4}$$

$$p_m^{(0)} = p_p^{(0)} \quad \text{on} \quad \Gamma_p. \tag{B.5}$$

This problem is formally identical to that of pressure diffusion in double porosity materials with highly-contrasted permeabilities[33,36]. Therefore, its solution is given by:

$$p_m^{(0)} = p_p^{(0)} \left(1 - \frac{j\omega \bar{b}(y,\omega)}{\mathcal{B}_{app}} \right), \tag{B.6}$$

where $\bar{b}(y,\omega)$ represents the Ω_p − periodic local diffusive pressure field and the apparent pressure diffusivity $\mathcal{B}_{app}$ is defined by:

$$\mathcal{B}_{app} = \frac{\mathcal{K}_m}{\eta \mathsf{C}_{mn}}. \tag{B.7}$$

The integration of the leading-order mass balance equation over the pore volume leads to:

$$j\omega \left\langle \frac{p_p^{(0)}}{P_0} - \frac{\tau_p^{(0)}}{\tau_0} \right\rangle + \nabla_x \cdot \langle \mathbf{u}_p^{(0)} \rangle + \langle \nabla_y \cdot \mathbf{u}_p^{(1)} \rangle = 0, \tag{B.8}$$

where the averaging operator is defined as:

$$\langle \cdot \rangle = \frac{1}{\Omega_p} \int_{\Omega_{pf}} \cdot \, d\Omega. \tag{B.9}$$

The last term on the left-hand side of Eq. (B.8) is calculated by i) using the divergence theorem, ii) taking into account that the surface integrals on opposite boundaries of the cell

cancel out due to periodicity and using Eq. (17) identified at order ϵ, iii) transforming the resulting surface integral into a volume integral using the divergence theorem, iv) integrating over the micro-nano porous domain the Eq. (15) identified at the dominant order, and v) replacing Eq. (B.6). The final result is:

$$\langle \nabla_y \cdot \mathbf{u}_p^{(1)} \rangle = j\omega p_p^{(0)} (1-\phi_p) \mathsf{C}_{mn}(\omega) \left(1 - \frac{j\omega B(\omega)}{(1-\phi_p)\mathcal{B}_{app}} \right), \tag{B.10}$$

where the inter-scale pressure diffusion function $B(\omega)$ is calculated as:

$$B(\omega) = \frac{1}{\Omega_p} \int_{\Omega_{mn}} \bar{b}(y,\omega) d\Omega. \tag{B.11}$$

The macroscopic description of sound propagation in multiscale sorptive materials, i.e. Eqs. (20) and (21), is then obtained by substituting Eqs. (B.10) and (B.3) into Eq. (B.8), using the thermodynamic identity $P_0/\tau_0 = \rho_0 C_p(\gamma-1)/\gamma$, and considering that the averaged fluid velocity is determined from Eq. (B.1), with the dynamic viscous permeability tensor being calculated as $\mathbf{k}_p(\omega) = \langle \bar{\mathbf{k}}_p(y,\omega) \rangle$. The dynamic thermal permeability associated to the pore scale is calculated as $\Theta_p(\omega) = \langle \bar{\theta}_p(y,\omega) \rangle$ (see Eq. (B.3)).

Appendix C

This appendix presents the derivation of the asymptotic values of effective dynamic compressibility $\mathsf{C}(\omega)$ given by Eqs. (30) and (31).

The behavior of $\mathsf{C}_i(\omega)$ (with $i = p, m$) is characterized by that of $\Theta_i(\omega)$, which is in turn determined by ω_{ti}. The thermal permeability varies[32] from $\Theta_i(\omega << \omega_{ti}) = \Theta_{i0}$ to $\Theta_i(\omega >> \omega_{ti}) = -j\phi_i\delta_t^2$, where $\delta_t = \sqrt{\kappa/\rho_0 C_p \omega}$ is the thermal boundary layer thickness. Therefore, the effective dynamic compressibility $\mathsf{C}_i(\omega)$ varies as[32]:

$$\mathsf{C}_i = \begin{cases} \frac{\phi_i}{P_0}\left(1 - \frac{\gamma-1}{\gamma}\frac{j\omega}{\omega_{ti}}\right) & \text{for} \quad \omega << \omega_{ti} \\ \frac{\phi_i}{\gamma P_0} & \text{for} \quad \omega >> \omega_{ti}. \end{cases} \tag{C.1}$$

The behavior of $\mathcal{F}_{mn}(\omega)$ is determined by that of $G(\omega)$. The latter is characterized by the mass diffusion characteristic frequency ω_d and varies[25] from $G(\omega << \omega_d) = G_0$ to $G(\omega >> \omega_d) = -j(1-\phi_m)\delta_d^2$, where $\delta_d = \sqrt{\mathcal{D}_{app}/\omega}$ is the mass diffusion boundary layer thickness. It then follows that $\mathcal{F}_{mn}(\omega << \omega_d) = 1 - j\omega/\omega_d$ and $\mathcal{F}_{mn}(\omega >> \omega_d) = 0$. Therefore, the effective dynamic compressibility C_{mn} takes the following asymptotic values:

$$\mathsf{C}_{mn} = \begin{cases} \frac{1}{P_0}\left(\phi_m + (1-\phi_m)H_e - j\omega\left(\frac{\gamma-1}{\gamma}\frac{\phi_m}{\omega_{tm}} + H_e\frac{(1-\phi_m)}{\omega_d}\right)\right) & \text{for} \quad \omega << \omega_d \\ \frac{\phi_m}{\gamma P_0} & \text{for} \quad \omega >> \omega_{tm}. \end{cases} \tag{C.2}$$

From Eq. (C.2), it is deduced that the static compressibility of the effective fluid saturating the micro-nano porous domain is given by[25] :

$$\mathsf{C}_{mn0} = \mathsf{C}_{mn}(\omega = 0) = \frac{\phi_m + (1-\phi_m)H_e}{P_0}. \tag{C.3}$$

The behavior of the function $\mathcal{F}_{pmn}(\omega)$ is determined by $B(\omega)$ and $\mathcal{B}_{app}(\omega)$. Focusing on isothermal sound propagation in the micropores (i.e. $\omega << \omega_{tm}$) and quasi-static inter-scale mass diffusion (i.e. $\omega << \omega_d$), the apparent pressure diffusivity is estimated by $\mathcal{B}_{app} \approx \mathcal{B}_{app0} = \mathcal{K}_{m0}/\eta\mathsf{C}_{mn0}$. Then, the pressure diffusion function varies from $B(\omega << \omega_b) = B_0$ to $B(\omega >> \omega_b) = -j(1-\phi_p)\delta_{b0}^2$, where $\delta_{b0} = \sqrt{\mathcal{B}_{app0}/\omega}$ is an estimation of the pressure diffusion boundary layer thickness. It then follows that $\mathcal{F}_{pmn}(\omega << \omega_b) = 1 - j\omega/\omega_b$ and $\mathcal{F}_{pmn}(\omega >> \omega_b) = 0$. Combining this result with Eqs. (22), (C.1), and (C.2), and only retaining linear terms in frequency, one obtains Eqs. (30) and (31).

REFERENCES

[1]D. Do, *Adsorption analysis: Equilibria and Kinetics* (Imperial College Press, 1998).

[2]H. Marsh and F. Rodriguez-Reinoso, *Activated Carbon* (Elsevier Science & Technology Books, 2006).

[3]S. M. Auerbach, K. A. Carrado, and P. K. Dutta, *Handbook of zeolite science and technology* (Marcel Dekker, Inc., 2003).

[4]G. Férey, "Hybrid porous solids: past, present, future." Chem. Soc. Rev. **37**, 191–214 (2008).

[5]J. Lewandowska, J. L. Auriault, S. Empereur, and P. Royer, "Solute diffusion in fractured porous media with memory effects due to adsorption." C. R. Mécanique. **330**, 879–884 (2002).

[6]D. Lydzba and J. L. Auriault, "Gas filtration through porous coal medium. Effect of the gas constrained in micropores." Arch. Mech. **48**, 447–473 (1996).

[7]F. Y. Wang, Z. H. Zhu, P. Massarotto, and V. Rudolph, "Mass transfer in coal seams for CO2 sequestration." AIChE Journal **53**, 1028–1049 (2007).

[8]T. D. Le, M. A. Murad, P. A. Pereira, and C. Boutin, "Bridging between macroscopic behavior of shale gas reservoirs and confined fluids in nanopores." Computat Geosci **20**, 751–771 (2016).

[9]M. Suzuki, *Adsorption Engineering* (Kodansha Ltd. and Elsevier Science, 1989).

[10]L. M. Naphtali and L. M. Polinski, "A novel technique for characterization of adsorption rates on heterogeneous surfaces." J. Phys. Chem. **67**, 369–375 (1963).

[11]Y. Yasuda, "Frequency response method for study of the kinetic behavior of a gas-surface system. 1. Theoretical treatment." J. Phys. Chem. **80**, 1867–1869 (1976).

[12]R. Song and L. V. C. Rees, "Frequency response measurements of diffusion in microporous materials." in *Adsorption and Diffusion, Molecular Sieves Science and Technology Vol. 7*, edited by H. G. Karge and J. Weitkamp (Springer, Berlin, 2008) pp. 235–276.

[13]E. Ruckenstein, A. S. Vaidyanathan, and G. R. Youagquist, "Sorption by solids with bidisperse pore structures." Chem. Eng. Sci. **26**, 1305–1318 (1971).

[14]K. Kawazoe, M. Suzuki, and K. Chihara, "Chromatographic study of diffusion in molecular sieve carbon." J. Chem. Eng. Japan **7**, 151–157 (1974).

[15]R. Jordi and D. D. Do, "Analysis of the frequency response method for sorption kinetics in bidispersed structured sorbents." Chem. Eng. Sci. **48**, 1103–1130 (1993).

[16]M. Nori and S. Brandani, "A model for sound propagation between two adsorbing microporous plates." J. Acoust. Soc. Am. **135**, 2634–2645 (2014).

[17]M. Nori, R. Venegas, and R. Raspet, "Acoustic frequency response method for the measurement of fast adsorption - diffusion processes. Theoretical treatment." Chem. Eng. Sci. **164**, 1–16 (2017).

[18]K. Herzfeld, "Reflection of sound." Phys. Rev. **53**, 899–906 (1938).

[19]J. G. Parker, "Effect of adsorption on acoustic boundary layer losses." J. Chem. Phys. **36**, 1547–1554 (1962).

[20]J. R. Wright, "The virtual loudspeaker cabinet." J. Audio Eng. Soc. **51**, 244–247 (2003).

[21]F. Bechwati, M. Avis, D. Bull, T. J. Cox, J. Hargreaves, D. Moser, D. Ross, O. Umnova, and R. Venegas, "Low frequency sound propagation in activated carbon." J. Acoust. Soc. Am. **132**, 239–248 (2012).

[22]R. Venegas, *Microstructure influence on acoustical properties of multiscale porous materials.*, Ph.D. thesis, University of Salford (2011).

[23]R. Venegas and O. Umnova, "Acoustical properties of double porosity granular materials." J. Acoust. Soc. Am. **130**, 2765–2776 (2011).

[24]R. Venegas and O. Umnova, "Influence of sorption on sound propagation in granular activated carbon." J. Acoust. Soc. Am. **140**, 755–766 (2016).

[25]R. Venegas and C. Boutin, "Acoustics of sorptive porous materials." Wave Motion **68**, 162–181 (2017).

[26]E. Sanchez-Palencia, *Non-Homogeneous Media and Vibration Theory* (Springer-Verlag, 1980).

[27]J. L. Auriault, C. Boutin, and C. Geindreau, *Homogenization of Coupled Phenomena in Heterogeneous Media* (ISTE Ltd and John Wiley & Sons, 2009).

[28]C. Boutin, "Sound propagation in rigid porous media : non-local macroscopic effects versus pores scale regime." Transp. Porous Med. **93**, 309–329 (2012).

[29]T. Levy and E. Sanchez-Palencia, "Equations and interface conditions for acoustic phenomena in porous media." J. Math. Anal. Appl. **61**, 813–834 (1977).

[30]J. L. Auriault, L. Borne, and R. Chambon, "Dynamics of porous saturated media, checking of the generalized law of Darcy." J. Acoust. Soc. Am. **77**, 1641–1650 (1985).

[31]D. L. Johnson, J. Koplik, and R. Dashen, "Theory of dynamic permeability and tortuosity in fluid-saturated porous media." J. Fluid Mech. **176**, 379–402 (1987).

[32]D. Lafarge, P. Lemarinier, J. F. Allard, and V. Tarnow, "Dynamic compressibility of air in porous structures at audible frequencies." J. Acoust. Soc. Am. **102**, 1995–2006 (1997).

[33]C. Boutin, P. Royer, and J. Auriault, "Acoustic absorption of porous surfacing with dual porosity." Int. J. Solids Struct. **35**, 4709–4737 (1998).

[34]I. Langmuir, "The constitution and fundamental properties of solids and liquids." J. Am. Chem. Soc. **38**, 2221–2295 (1916).

[35]J. F. Allard and N. Atalla, *Propagation of Sound in Porous Media: Modeling Sound Absorbing Materials* (John Wiley & Sons, 2009).

[36]X. Olny and C. Boutin, "Acoustic wave propagation in double porosity media." J. Acoust. Soc. Am. **113**, 73–89 (2003).

[37]V. F. Kozlov, A. V. Fedorov, and N. D. Malmuth, "Acoustic properties of rarefied gases inside pores of simple geometries." J. Acoust. Soc. Am. **117**, 3402–3411 (2005).

[38]C. Boutin and C. Geindreau, "Estimates and bounds of dynamic permeability of granular media." J. Acoust. Soc. Am. **124**, 3402–3411 (2008).

[39]C. Boutin and C. Geindreau, "Periodic homogenization and consistent estimates of transport parameters through sphere and polyhedron packings in the whole porosity range." Phys. Rev. E **82**, 036313 (2010).

[40]O. Umnova, D. Tsiklauri, and R. Venegas, "Effect of boundary slip on the acoustical

properties of microfibrous materials." J. Acoust. Soc. Am. **126**, 1850–1861 (2009).

[41]BS EN 29053:1993, "Acoustics. Materials for acoustical applications. Determination of airflow resistance," Standard (British Standards Institute, 1993).

[42]ISO 10534-2:2001, "Acoustics–Determination of sound absorption coefficient and impedance in impedance tubes–Part 2: Transfer-function method," Standard (International Organization for Standardization, 2001).

[43]S. A. Al-Muhtaseb, F. A. A. Al-Rub, and M. A. Zarooni, "Adsorption equilibria of nitrogen, methane, and ethane on BDH-activated carbon." J. Chem. Eng. Data **52**, 60–65 (2007).

[44]Y. H. Ma, W. Sun, M. Bhandarkar, J. Wang, and G. W. Miller, "Adsorption and diffusion of nitrogen, oxygen, argon, and methane in molecular sieve carbon at elevated pressures." Separ. Technol. **1**, 90–98 (1991).

[45]B.-U. Choi, D. K. Choi, Y. W. Lee, B. K. Lee, and S. H. Kim, "Adsorption equilibria of methane, ethane, ethylene, nitrogen, and hydrogen onto activated carbon." J. Chem. Eng. Data **47**, 603–607 (2003).

[46]Y. D. Chen, R. T. Yang, and P. Uawithya, "Diffusion of oxygen, nitrogen and their mixtures in carbon molecular sieve." AIChE Journal **40**, 577–585 (1994).

[47]K. Chihara, M. Sukuzi, and K. Kawazoe, "Adsorption rate on molecular sieving carbon by chromatography." AIChE Journal **24**, 237–245 (1978).

[48]R. P. Ribeiro, T. P. Sauer, F. V. Lopes, R. F. Moreira, C. A. Grande, and A. E. Rodrigues, "Adsorption of CO2, CH4, and N2 in activated carbon honeycomb monolith." J. Chem. Eng. Data **53**, 2311–2317 (2008).

[49]F. Brandani, A. Rouse, S. Brandani, and D. M. Ruthven, "Adsorption kinetics and dynamic behavior of a carbon monolith." Adsorption **10**, 99–109 (2004).

[50]C. Shen, *Rarefied Gas Dynamics, Fundamentals, Simulations and Micro Flows* (Springer-Verlag, 2005).

[51]J. C. Maxwell, "On stresses in rarefied gases arising from inequalities of temperature." Philos. Trans. R. Soc. Part 1 **170**, 231–256 (1879).

[52]M. V. Smoluchowski, "Ueber wärmeleitung in verdünnten gasen." Ann. Phys. Chem. **64**, 101–130 (1898), (On conduction of heat by rarefied gases).

[53]J. Chastanet, P. Royer, and J. L. Auriault, "Acoustics with wall-slip flow of gas saturated porous media." Mech. Res. Commun. **31**, 277–286 (2004).